

**UNCLASSIFIED**

---

**AD 274 624**

*Reproduced  
by the*

**ARMED SERVICES TECHNICAL INFORMATION AGENCY  
ARLINGTON HALL STATION  
ARLINGTON 12, VIRGINIA**



---

**UNCLASSIFIED**

## **DISCLAIMER NOTICE**

**THIS DOCUMENT IS BEST QUALITY  
PRACTICABLE. THE COPY FURNISHED  
TO DTIC CONTAINED A SIGNIFICANT  
NUMBER OF PAGES WHICH DO NOT  
REPRODUCE LEGIBLY.**

NOTICE: When government or other drawings, specifications or other data are used for any purpose other than in connection with a definitely related government procurement operation, the U. S. Government thereby incurs no responsibility, nor any obligation whatsoever; and the fact that the Government may have formulated, furnished, or in any way supplied the said drawings, specifications, or other data is not to be regarded by implication or otherwise as in any manner licensing the holder or any other person or corporation, or conveying any rights or permission to manufacture, use or sell any patented invention that may in any way be related thereto.

62-5-2

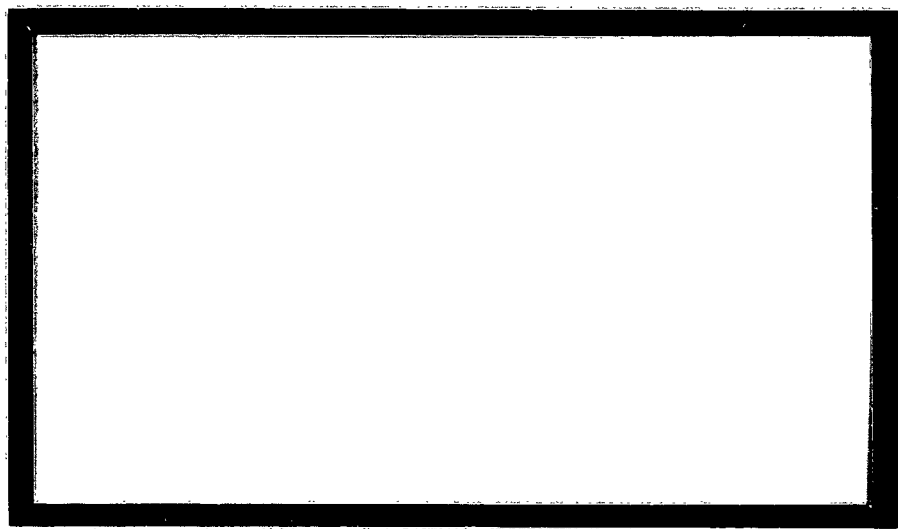
274624

CATALOGED BY  
AS AD 140.

274 624

# University of Utah

## Department of Chemical Engineering



Salt Lake City, Utah

908 100

UNIVERSITY OF UTAH

DEPARTMENT OF CHEMICAL ENGINEERING

AFOSR 2225

Final Technical Report

on

IGNITION AND COMBUSTION OF SOLID PROPELLANTS

Under Contract AF 49(638)-170

March, 1957 to September 30, 1961

Report prepared by:

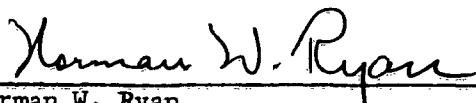
Rex C. Mitchell

John A. Keller

Alva D. Baer, Investigator

Norman W. Ryan, Principal Investigator

Report approved by:

  
Norman W. Ryan

# TABLE OF CONTENTS

PART	PAGE
SUMMARY . . . . .	1
I. INTRODUCTION . . . . .	2
II. PROPELLANT IGNITION BY THERMAL RADIATION . . . . .	3
Introduction and Theory . . . . .	3
Apparatus and Procedure . . . . .	8
Results of Radiation Furnace Tests . . . . .	11
Atmospheric Pressure Tests . . . . .	11
Ignition Tests at Non-Atmospheric Pressure . . . . .	13
The Effect of Long-Time Storage . . . . .	16
Conclusions . . . . .	16
III. PROPELLANT IGNITION IN THE SHOCK TUBE . . . . .	18
Introduction . . . . .	18
Apparatus and Procedure . . . . .	18
Results . . . . .	24
Conclusions . . . . .	29
IV. EXPLORATORY STUDIES . . . . .	30
Diffusion Flame Experiments . . . . .	30
Effect of Pressure Changes on Burning Propellant . . . . .	31
Flame Spread . . . . .	33
APPENDIX A - HEAT TRANSFER . . . . .	36
APPENDIX B - RAREFACTION TUBE THEORY . . . . .	43
APPENDIX C - TABLES . . . . .	54
TABLE OF NOMENCLATURE . . . . .	75
LIST OF REFERENCES . . . . .	77

# LIST OF FIGURES

FIGURE	PAGE
1. Sectional View of the Sealed, Low Temperature Furnace . . . . .	9
2. Sample Mounting for the Radiation Furnace . . . . .	10
3. Ignition Data From Radiation Furnace Tests . . . . .	12
4. Effect of Initial Propellant Temperature on Ignition Times . . . .	14
5. The Effect of Furnace Pressure on the Ignition Times of A and D Propellants . . . . .	15
6. Schematic Diagram of Shock Tube . . . . .	19
7. Test Section . . . . .	20
8. Propellant Sample Holder . . . . .	21
9. Ignition-Test Oscilloscope Traces . . . . .	23
10. Ignition Time Versus Heat Flux A Propellant . . . . .	25
11. Ignition Time Versus Heat Flux B Propellant . . . . .	25
12. Ignition Time Versus Heat Flux C Propellant in Air 3/8" Orifice .	26
13. Ignition Time Versus Heat Flux C Propellant in Air 5/16" Orifice .	26
14. Ignition Time Versus Heat Flux C Propellant in Air 1/4" Orifice .	27
15. Ignition Time Versus Heat Flux C Propellant in Nitrogen . . . . .	27
A-1. Correlation of the Initial Discontinuous Surface Temperature Rise of the Heat Flux Gages with the Shock Mach Number at End of the Shock Tube . . . . .	38
A-2. Heat Transfer Coefficients to the Walls of the Various Shock Tube Test Sections . . . . .	40
B-1. Wave Diagram for Rarefaction Tube . . . . .	44

Stark

## SUMMARY

This report summarizes work performed under AFOSR Contract AF 49(638)-170 with the University of Utah. The project was activated early in 1957 and terminated September 30, 1961. The original objective, to study the ignition of composite propellants, was broadened to encompass the study of other combustion transients, these being, so far, subjected only to exploratory investigation. All phases of the work are still in progress under Air Force Grant AF AFOSR 62-99.

The study of ignition was concerned with the response of propellant to externally supplied heat flux. Both radiant flux from electrically heated tube furnaces and convective flux from shock-heated gas were employed, the former giving fluxes in the range 5 to 50, the latter, 100 to 300 Btu per sec., sq. ft. The results, ignition delay time as a function of heat flux are correlated, ~~by a modified form of the theory originally set forth by B. L. Hicks [4],~~ according to which the ignition delay time should be nearly proportional to the square of the heat flux. The extent of deviation from proportionality provides a measure of kinetic parameters.

The theory ~~predicts~~ predicts the effect of initial propellant temperature on the ignition time-heat flux relationship, but is non-committal with respect to the effect of pressure. ~~Empirically it is found that~~ the effect of pressure on the ignition delay time of perchlorate propellants is a function of heat flux level, being very slight, for the propellants studied, at flux levels above 20 Btu per sec., sq.ft.

Exploratory studies ~~also~~ concerned flame spread, effects of aerodynamic transients on burning propellant, and the diffusion flame between large bodies of fuel and oxidant. One firm conclusion is that flame spread across fresh surface, unassisted by external heat flux to that surface, is too slow to be an important factor in the overall ignition process. As one aspect of the aerodynamic transient studies, a theory of the rarefaction tube was developed, ~~and is here presented.~~

↑

- 1 -



## I. INTRODUCTION

Research on the combustion transients of solid rocket propellants was begun at the University of Utah early in 1957, under sponsorship of the U.S. Air Force Office of Scientific Research, Contract AF 49(638)-170. This is a final technical report on the work under that contract, three times extended to a final termination date of 30 September, 1961. It will be noted that several phases of the study are not complete, these being still in progress under Air Force Grant AF-AFOSR 62-99.

The limited objective originally conceived was to study ignition of propellants mounted in a shock tube. It was soon discovered, however, that properly restricted samples, when mounted in the tube wall, could not be ignited except by chemical participation of the shock-heated environmental gas. Such ignition was judged unrealistic from the point of view of rocket ignition practice. Consequently a technique was developed which employed the shock tube as a generator for hot gas, subsequently used as a source of convective heat at high, sustained flux levels.

Adoption of the technique of high convective flux required an extensive auxiliary study of heat transfer, this study in turn requiring the development of ceramic-backed thin-film platinum resistance thermometers as fast-response heat-flux gages.

To supplement the primary study with high convective flux, a second ignition study employing black-body radiative flux was conducted. At the lower flux levels interesting effects of pressure and initial propellant temperature have been observed.

Other studies, briefly pursued, have been of the diffusion flame between large bodies of ammonium perchlorate and fuel-binder, of the effect of shock and rarefaction waves on burning propellant surface, and of flame spread over fresh propellant surface.

In order of presentation, ignition by radiative flux is discussed first (Section II). Section II contains an outline of heating and ignition theory as employed throughout the study. Ignition by convective flux is discussed next (Section III). Then the peripheral exploratory studies are discussed (Section IV). Much of the detail, including a discussion of rarefaction theory, is placed in the Appendix.

## II. PROPELLANT IGNITION BY THERMAL RADIATION

### Introduction and Theory.

A very convenient technique for the study of ignition of solid propellants is to subject the propellant surface to a thermal radiation flux of known intensity and to photoelectrically measure the time until a flame appears. The virtues of the technique are: (1) the propellant surface can be viewed and the first signs of ignition and flame detected easily, (2) the propellant can be exposed to reducing or oxidizing gases under pressure or vacuum independent of the energy source, and (3) if black-body conditions are approached by the energy source, the propellant emissivity is high and its transmissivity low, the radiant heat flux and variations in heat flux may be accurately calculated. Also, the propellant surface is not disturbed by the flow of gas past the surface, as is the case of convective heat transfer is employed. Unfortunately, with simple apparatus it is difficult to obtain very high radiant heat fluxes, and propellant ignition times much less than one-half second are not normally feasible. The relatively complicated arc-image furnace employed by Fishman and Beyer [1] does produce radiant fluxes comparable to those found in igniter practice [2]. In the present study, two simple tube furnaces were constructed to serve as black body sources of radiation. An atmospheric furnace capable of operation up to 1780°K and a sealed pressure or vacuum furnace capable of operation up to 1350°K were used.

Altman [3] was probably the first to show experimentally that the ignition time of a solid propellant can be calculated from unsteady-state heat-transfer theory in terms of a characteristic ignition temperature. This surface ignition temperature ( $T_{si}$ ) was calculated for the observed ignition time,  $\theta_i$ , assuming the propellant to be a chemically passive solid of constant density, heat capacity, and thermal conductivity.

Hicks showed that  $T_{si}$  should be a weak function of the surface heat flux. He considered an ignition model in which only exothermic, exponentially-temperature-dependent propellant reactions are considered. One dimensional heat flow for this model related the propellant temperature ( $T$ ) to position ( $x$ ) and time ( $\theta$ ) by the following non-linear differential equation:

$$\rho c \frac{\partial T}{\partial \theta} = k \frac{\partial^2 T}{\partial x^2} + B q' e^{-\frac{E}{RT}} \quad (1)$$

where  $k$ ,  $\rho$ , and  $c$  are respectively the propellant thermal conductivity, density and heat capacity,  $B$  is a constant describing the reaction rate,  $q'$  is the energy generated per unit volume by the reaction and  $E/R$  is the propellant reaction activation energy divided by the gas constant. Hicks obtained numerical solutions to Equation (1) for semi-infinite slabs heated at the surface. The end of the ignition period was taken to be the time when the calculated surface temperature reached an assigned value. For the case in which the surface heat flux is maintained until ignition occurs, he found that the ratio of the rate of energy generation at the surface by exothermic reaction to the rate of energy absorption at the surface for linear heating (no reaction) was a constant at ignition time. This concept leads to the criterion that ignition occurs when the ratio

$$I = \frac{B q' e^{-\frac{E}{RT_{si}}}}{\rho c \left( \frac{\partial T_s}{\partial \theta} \right)_i} \quad (2)$$

is a known constant.  $T_s$  is the linearly estimated surface temperature and the subscript  $i$  denotes evaluation at  $\theta_i$ . If  $I$  is characteristic of a propellant, it has been shown [5] that

$$\left( \frac{\partial \ln \theta_i^{1/2}}{\partial \ln f_s} \right)_{T_0} = S = - \frac{\frac{E}{R}(T_{si} - T_0) - T_{si}^2}{\frac{E}{R}(T_{si} - T_0) + T_{si}^2} \quad (3)$$

Since  $S$  is found to be essentially independent of  $T_{si}$ , a plot of  $\log \theta_i^{1/2}$  versus  $\log f_s$  should be a straight line of slope slightly greater than minus one. Experimentally it is found that for a series of tests, the value of  $T_{si}$  computed from heat-flux data increases as the surface heat flux is increased. The criterion indicated by Equation (2) predicts this effect.

For a constant surface heat flux, the linearly estimate surface temperature ( $T_{si}$ ) can be calculated since

$$T_s - T_0 = \frac{2 f_s}{\Gamma} \left( \frac{\theta}{\pi} \right)^{1/2} \quad (4)$$

where  $T_0$  is the initial, uniform propellant temperature and  $\Gamma = \sqrt{k\rho c}$  for the propellant. For a single ignition test with  $T_0$  and  $f_s$  constant, Equations (2) and (4) can be combined to show that

$$\left( \frac{\partial T_s}{\partial \theta} \right)_i = \frac{f_s}{\Gamma (\pi \theta)^{1/2}} = \frac{B q'}{\rho c I} e^{-\frac{E}{RT_{si}}} \quad (5)$$

If Equations (4) and (5) are put into a logarithmic form and differentiated with respect to  $T_0$  for constant  $f_s$ , the resulting equations can be combined and simplified to give the following result:

$$\left( \frac{\partial T_{si}}{\partial T_0} \right)_{f_s} = \frac{1}{1 + \frac{E}{R} \frac{T_{si} - T_0}{T_{si}^2}} \quad (6)$$

If Equation (4) is differential with respect to  $T_0$  for constant  $f_s$ , it is found that at  $\theta_i$

$$\left( \frac{\partial \theta_i^{1/2}}{\partial T_0} \right)_{f_s} = \frac{\sqrt{\pi} \Gamma}{2 f_s} \left[ \left( \frac{\partial T_{si}}{\partial T_0} \right)_{f_s} - 1 \right] \quad (7)$$

The significance of Equations (5), (6), and (7) will be discussed later.

The Hicks model considers homogeneous reaction throughout the propellant; the non-linear temperature dependent term occurs in the differential equation. While a homogeneous reaction probably occurs in a double-base propellant, the important reactions in the ignition of the heterogeneous composite propellants probably occur near or at the surface. Gas phase reactions may also be important. If an ignition model is assumed which involves only an exothermic, exponentially-temperature-dependent surface reaction and passive response of the bulk of the propellant, the differential equation relating temperature, position, and time is the normal one-dimensional heat conduction equation.

$$\frac{\partial T}{\partial \theta} = \frac{k}{\rho c} \frac{\partial^2 T}{\partial x^2} \quad (8)$$

The boundary condition at  $x = 0$  is

$$-k \frac{\partial T}{\partial x} = f_s + A f' e^{-\frac{E}{RT}}$$

where  $f_s$  is the externally imposed surface heat flux,  $A$  is a constant describing the reaction rate, and  $f'$  is the energy generated per unit area at the surface by reaction. By analogy to the relationship between Equation (1) and (2), it is anticipated that ignition times can be calculated by use of Equation (8) and the criterion defined by Equation (9) for constant values of  $H$ .

$$H = \frac{A f' e^{-\frac{E}{RT_{si}}}}{f_{si}} \quad (9)$$

where  $T_{si}$  is calculated by neglecting propellant reactions.  $A$  is proportional to the energy generated per unit surface area,  $f_{si}$  the surface heat flux at the ignition time, and  $E$  the activation energy of the rate limiting surface reaction.

The rate-limiting reaction may be endothermic. Evenso, if it is followed immediately by a rapid and strong exothermic reaction, the net effect would be that of an exothermic reaction and the energy generation factor A would be positive. The criterion defined by Equation (9) can be checked by numerical calculations for the assumed ignition model of a passive semi-infinite body with an exponentially temperature dependent surface reaction. For this criterion, a development similar to that leading to Equation (3) gives

$$\left( \frac{\partial \ln \theta_i^{1/2}}{\partial \ln f_s} \right)_{T_0} = \mathcal{S} = -1 + \frac{T_{si}^2}{\frac{E}{R} (T_{si} - T_0)} \quad (10)$$

Again it is indicated that a plot of  $\log \theta_i^{1/2}$  versus  $\log f_s$  should be a straight line of slope slightly greater than minus-one. For a given slope,  $\mathcal{S}$ , the E/R values are about one-half the E/R values for the same slope, S, evaluated from Equation (3).

Since Equation (9) implies that  $T_{si}$  is not a function of  $T_0$ , the initial propellant temperature,

$$\left( \frac{\partial T_{si}}{\partial T_0} \right)_{f_s} = 0 \quad (11)$$

If Equation (11) is substituted into Equation (7), it is found

$$\left( \frac{\partial \theta_i^{1/2}}{\partial T_0} \right)_{f_s} = - \frac{\sqrt{\pi} \Gamma}{2 f_s} \quad (12)$$

The criteria indicated by Equations (2) and (9) can only apply when the external surface heat flux is maintained up to the ignition time. In the tests discussed here, this requirement was met. It is anticipated that propellant ignition can be characterized by the linearly estimated surface temperature at ignition ( $T_{si}$ ) for one surface heat flux, the limiting activation energy (E/R) and the thermal properties of the propellant ( $\Gamma$ ). Such an approach should yield useful information in a practical form much sooner than could be realized by a detailed study of the chemistry.

### Apparatus and Procedure.

The atmospheric furnace and the sealed pressure-vacuum furnace used in this study were identical in principle of operation, and ignition results from the two furnaces were in good agreement. The atmospheric furnace is described in detail in previous reports [5], [6]. A diagrammatic sketch of the sealed furnace is shown in Figure 1. The furnace-core dimensions were the same as for the atmospheric furnace. A photo conductivity crystal mounted to view a narrow angle down the axis of the furnace was used to detect ignition.

Cut discs of propellant were mounted in sample holders, the irregular edges of the discs were covered by aluminum-foil washers and the sample holders were mounted in an injection holder. Figure 2 illustrates the method of supporting the sample before injection into the furnace. The injection holder was pushed into the furnace on the end of a long rod. Initially this rod was driven by a long solenoid. The stainless-steel core of the solenoid was at furnace pressure. In later tests, the rod was driven manually through o-ring seals. As the injection holder was pushed into the furnace, the surface of the sample was protected from radiation by a foil shield. When the injection mechanism reached the end of its travel, inertia carried the sample holder through the foil shield and exposed the propellant surface to radiation (Figure 2). Tests showed that the time required to expose the propellant completely was 20-30 msec. The time interval between the injection mechanism first reaching the end of its travel and the first light signal detected by the photo conductivity crystal was taken to be the ignition time.

Atmospheric and vacuum tests were made in air since it was determined that the atmospheric oxygen did not affect the ignition [6]. Tests at pressures greater than atmospheric were made with nitrogen in the furnace. Normally the propellant was initially at ambient temperature. For some tests the initial temperature was intentionally varied, and the injection holders (inside sealed, insulated tubes) were held in an oven or a cold-chest several hours before each run. Some condensation of atmospheric water vapor on the injection holder occurred for tests at -30 and -60°C. Careful shielding and rapid handling minimized condensation on the propellant surface. In all tests, freshly cut surfaces of propellant were exposed to the radiation.

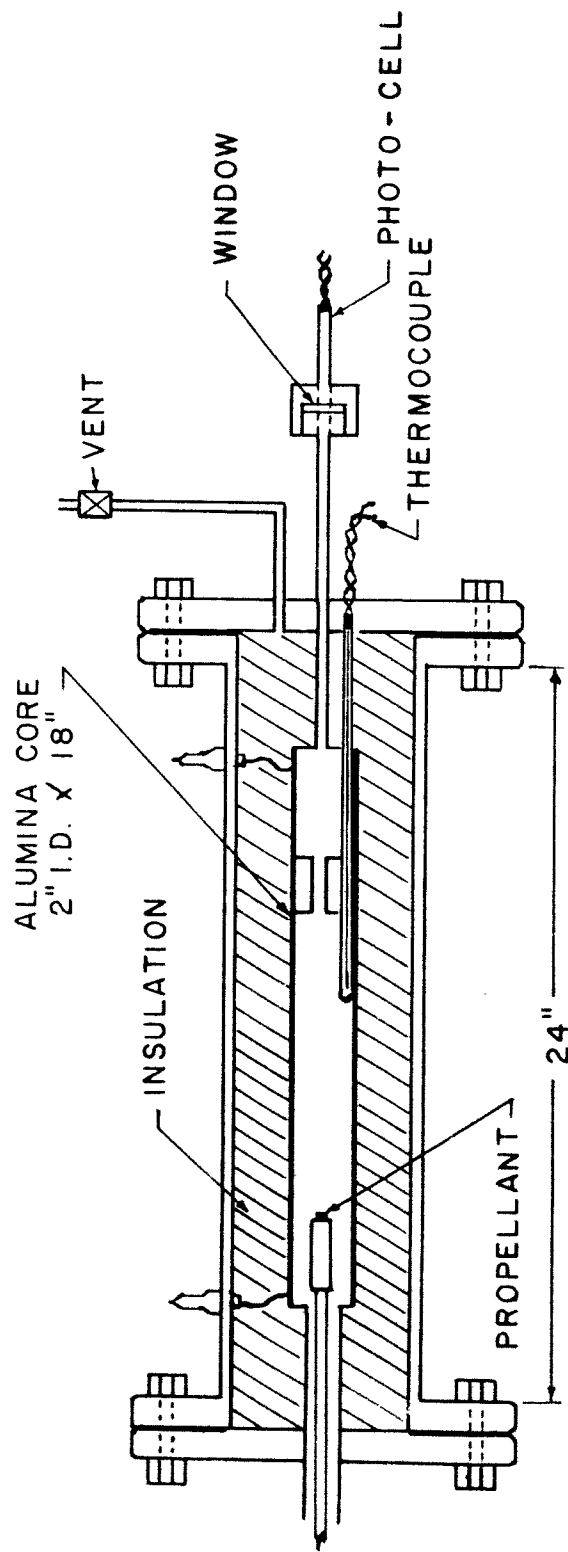


Figure 1. Sectional view of the low-temperature radiation furnace. The furnace body is standard 2-in. pipe welded to 300 lb. flange-end. The 2-in. long furnace core is wrapped with foil. Propellant samples, in holders and covered by an aluminum foil shield, are pushed rapidly into the furnace from the left end of the furnace and are stopped in the position shown after the inertia of the sample holder forces aside the foil shield. See Figure 2.





Figure 2. Sample Mounting for the Radiation Furnace.

On the right the propellant sample is shown mounted in the sample holder. In the middle the aluminum washer is shown in position to protect the sample edge. On the left the sample holder, in the injection holder, is shown after having forced aside the aluminum foil radiation shield.

### Results of Radiation Furnace Tests.

Four commercial propellants, three containing ammonium perchlorate and one containing ammonium nitrate, were used in this study. These same propellants, designated A, B, C, and D were used in previously reported work [5], [6], and [7]. Table II summarizes the pertinent physical and ballistic properties of these propellants. This work extended over a three year period; as explained later, some effect of aging of sealed samples was observed. All data are summarized in Tables II to VIII.

### Atmospheric Pressure Tests.

Atmospheric tests (12.6 psia) were made on all four propellants in the high temperature furnaces. Figure 3 shows a plot of  $\log \theta_i^{\frac{1}{2}}$  versus the logarithm of the furnace heat flux for all tests. In each case the slopes of these lines are slightly greater than minus one as predicted by Equation (3). Activation energies (E/R) calculated from these slopes and Equation (3) were approximately 30,000°K for the perchlorate propellants and 15,000°K for the nitrate propellant. Additional tests were made on the A propellant in which the initial propellant temperature was -60, -30, 0, 30, and 60°C. If a value for E/R of 30,000°K is taken for this propellant, Equation (6) indicates that

$$\left( \frac{\partial T_{si}}{\partial T_o} \right)_{f_s} \approx 0.04$$

For the 120°C variation in the initial propellant temperature, Equation (6) indicates that  $T_{si}$  should vary only 5°C. Equation (11) predicts that  $T_{si}$  is independent of  $T_o$ . Calculated values of  $T_{si}$  appear in Table IV. Within the experimental error,  $T_{si}$  is seen to be independent of  $T_o$ . This result is useful since it shows that ignition data obtained at one initial propellant temperature can be used to predict ignition times for different initial propellant temperatures.

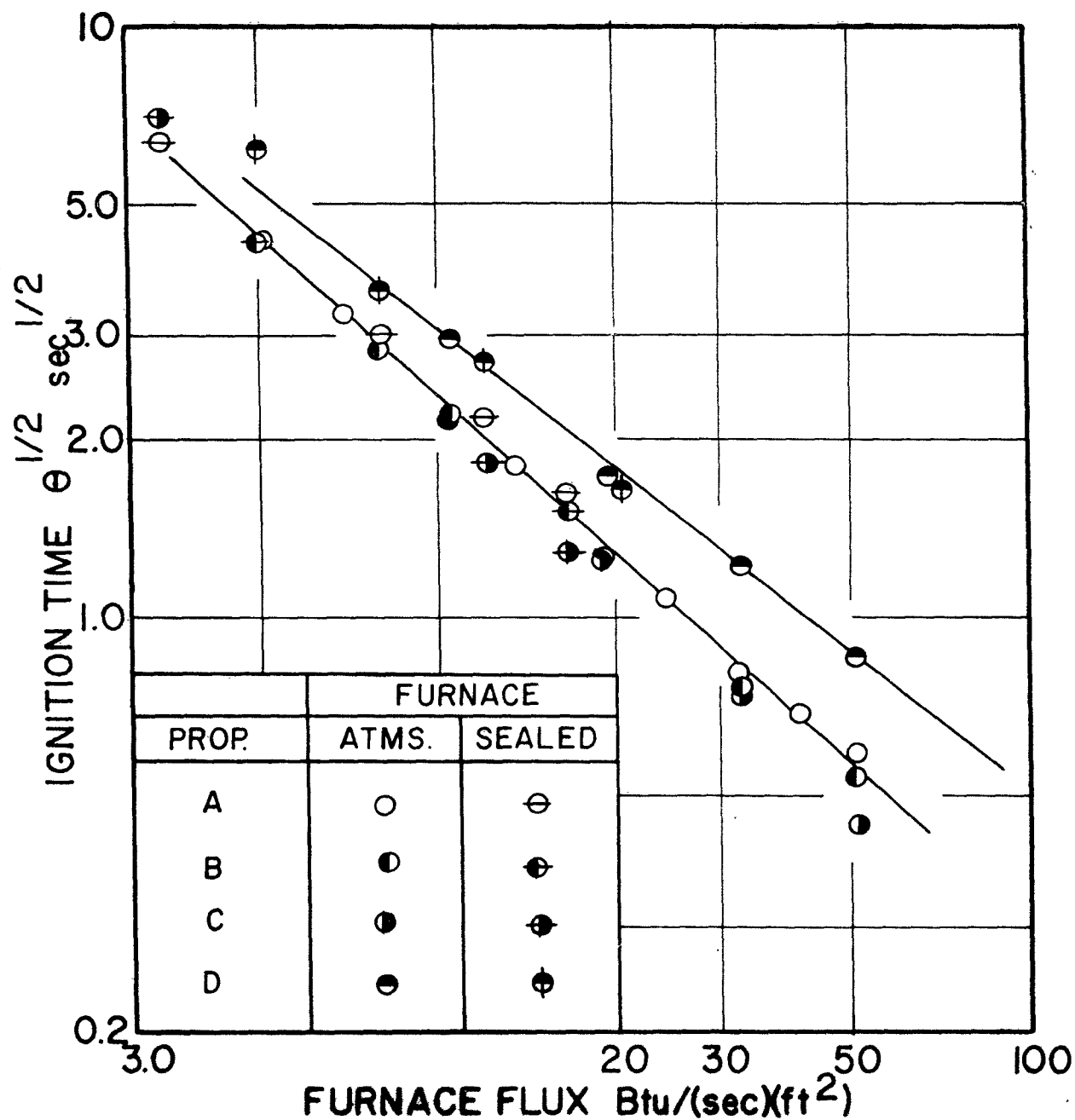


Figure 3. Ignition Data From Radiation Furnace Tests Plotted as Suggested by Equations 3 and 10. All tests were at 0.25 atm. pressure.

Equation (12) indicates that a plot of  $\theta_i^{\frac{1}{2}}$  versus  $T_o$  should be a straight line and that the true surface heat flux can be calculated from the slope of this line and the thermal responsivity ( $\Gamma$ ) of the propellant. For practical values of the parameters, essentially the same result is indicated by Equation (7). For a value of  $\Gamma = 2.64 \text{ Btu/hr } 1/2 \text{ ft}^2 \text{ } ^\circ\text{F}$  for the A propellant,  $f_s$  is found to be 92 per cent of the flux calculated for black-body furnace conditions. This value is reasonable for the radiation absorptivity of the surface.

The slopes of all lines shown in Figure 4 are compatible with this same value of absorptivity. Thus Equation (7) and (12) predict a surface heat flux in agreement with the independently measured furnace temperature.

#### Ignition Tests at Non-Atmospheric Pressures.

Tests at pressures other than atmospheric were made in the sealed, low temperature furnace. Figure 5 shows a plot of data for the A and D propellants. Tests at 0.85, 2.55, and 4.25 standard atmospheres were made with the D propellant. The ignition time of this nitrate propellant appears to be a strong function of pressure at pressures below atmospheric and to be essentially independent of pressure at pressures much greater than atmospheric. This result essentially confirms the data reported by Fishman and Beyer [1]. All the perchlorate based propellants indicated the same ignition time dependence on pressure as shown for the A propellant in Figure 5, or

$$\theta_i \propto p^{-n}$$

(13)

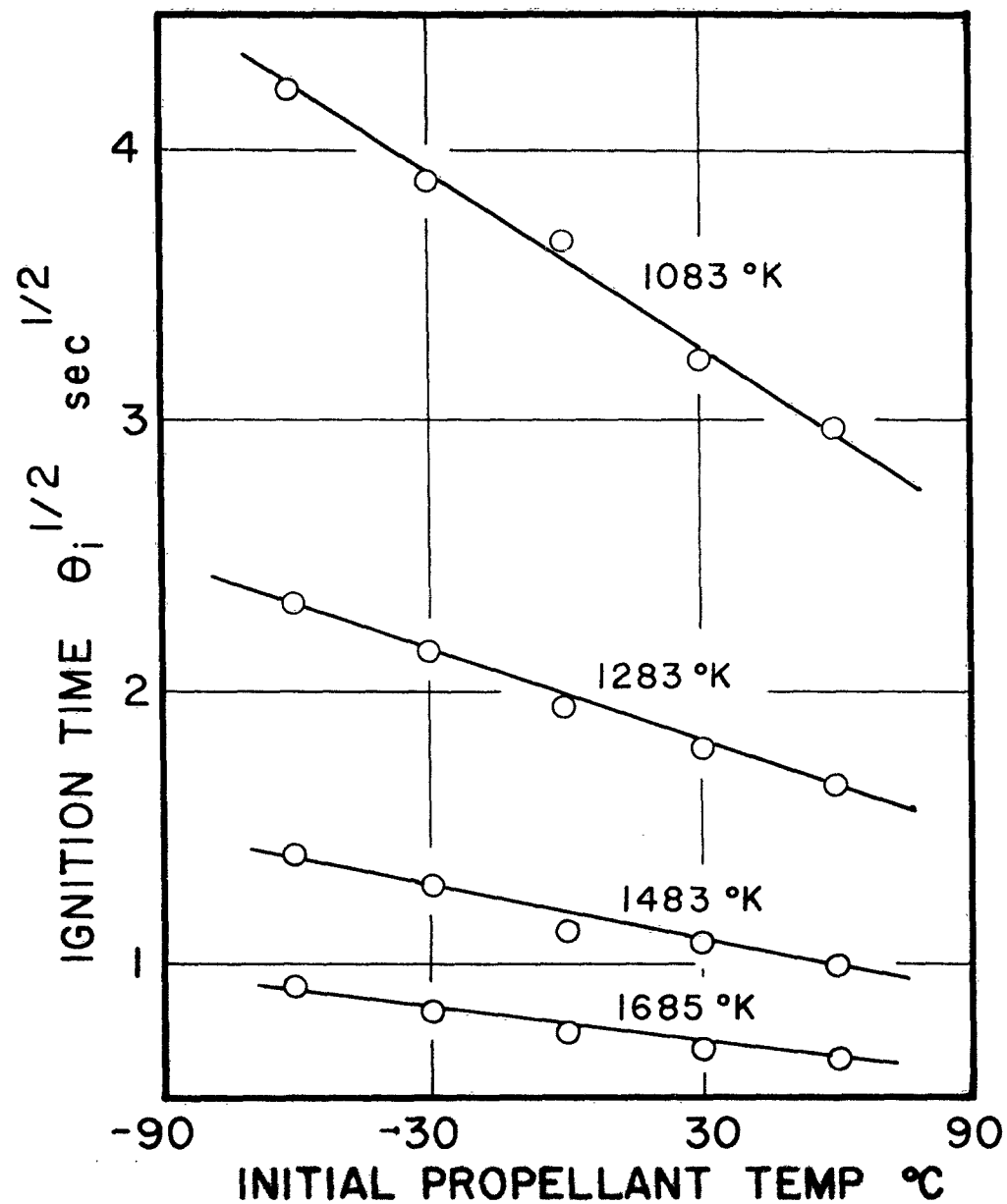
where  $p$  is the furnace pressure. These results are summarized in Table I.

TABLE NO. I

#### THE EFFECT OF PRESSURE ON THE IGNITION TIMES OF AMMONIUM PERCHLORATE BASED PROPELLANTS

The Values of  $n$  Defined as  $\theta_i \propto p^{-n}$   
Are Tabulated as a Function of Furnace Temperature

Propellant	Radiation Furnace Temperature $^{\circ}\text{K}$				
	908	1000	1125	1248	1347
A	0.22	n.d.	0.18	0.19	0.12
B	n.d.	0.12	0.11	n.d.	0.10
C	0.13	n.d.	0.045	0.00	0.00



**Figure 4.** Effect of Initial Propellant Temperature on Ignition Times. The data are plotted as suggested by Equations 7 and 12. The slope of each time was calculated from these equations for a surface heat flux 90 per cent of the black body flux corresponding to the indicated furnace temperature.

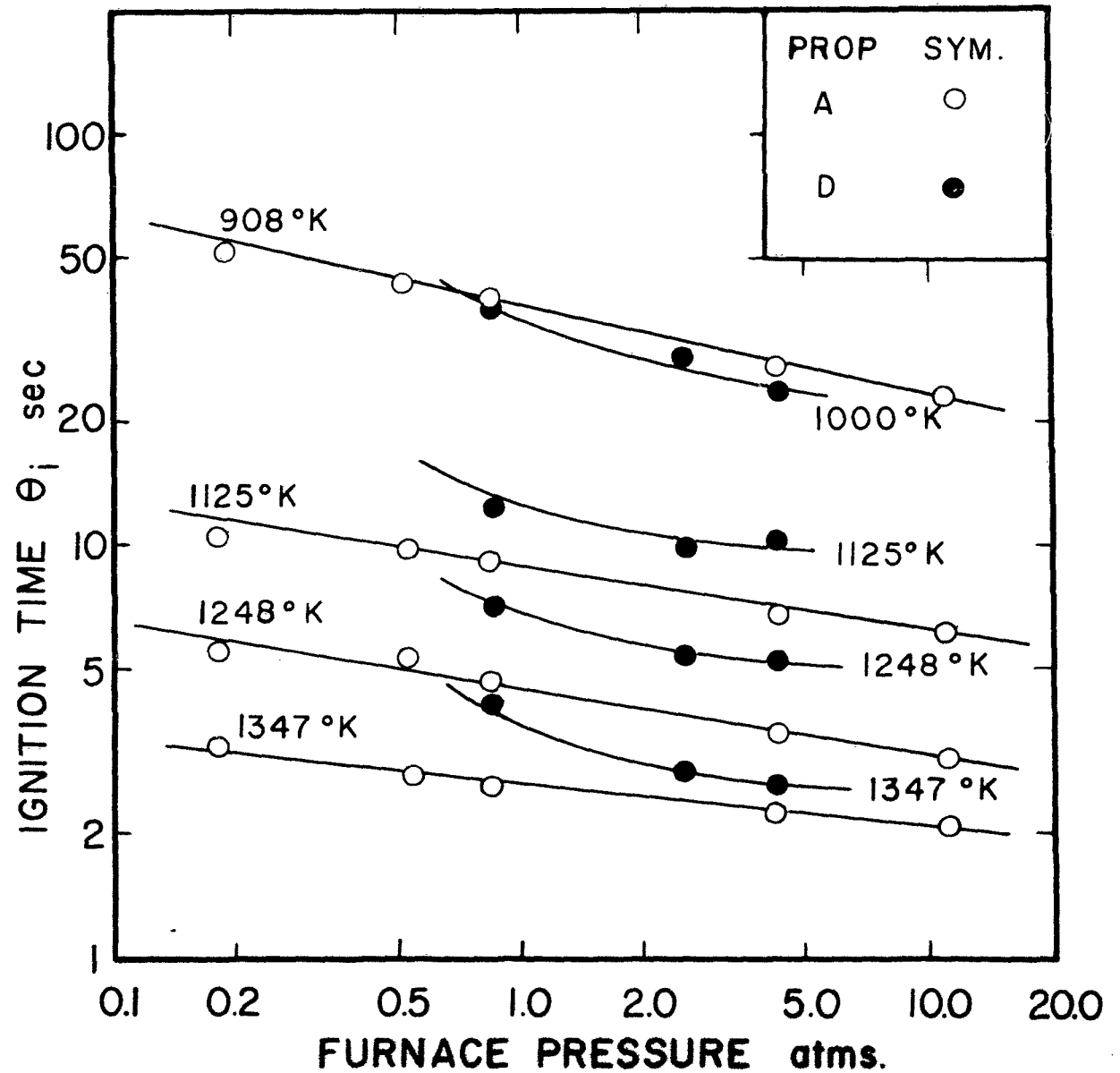


Figure 5. The Effect of Furnace Pressure on the Ignition Times of A and D Propellants. The lines are labeled corresponding to the furnace temperature.

In each case the ignition time appears to approach independence of pressure as the surface heat flux increases. For the three perchlorate propellants tested, the ignition times should be pressure independent for the normal igniter heat fluxes, at least for pressures greater than 0.2 atms.

#### The Effect of Long-Time Storage.

The effect of aging on the ignition times of these propellants is illustrated at atmospheric pressure by the data summarized in Figure 3. The earliest tests in the high temperature, atmospheric furnace were made three years prior to the tests made in the low temperature, sealed furnace. All propellant samples were held in sealed plastic bags at ambient temperature during this period. Samples surfaces were cut from the interior of stored slabs. Within the experimental error, it appears that storage produced negligible effect on the ignition times for the B, C, and D propellants. The A propellant showed an apparent increase in ignition time of a few per cent during the three-year storage period. Visible discoloration of this propellant occurred during the storage.

#### Conclusions.

Although these tests have not produced ignition data directly applicable to high-flux ignition systems, several effects were noted which can probably be extrapolated beyond the range of the data.

1. The concept of a linearly estimated propellant surface temperature at ignition appears to be very useful. Equations (3) and (6), or (10) and (11), quantitatively predict the effects of surface heat flux and initial propellant temperature on ignition times. Surface heat fluxes calculated from the effect of initial propellant temperature on the ignition times and the thermal propellant properties (Equations (7) or (12)) are in good agreement with the surface fluxes calculated from only thermal radiation heat transfer considerations.
2. The effect of pressure on the ignition times of the ammonium perchlorate based propellants was represented by an equation of the form of Equation (13). As the surface heat flux is increased,  $n$  approached zero and the ignition times became independent of pressure.

3. At high pressures, it appears to be possible to completely characterize the ignition properties of an ammonium perchlorate in terms of the surface ignition temperature at one surface heat flux and the activation energy of the ignition limiting reactions. Since this ignition temperature did not change greatly for different ammonium perchlorate propellants, it appears to be possible to develop adequate approximate methods for predicting the changes in this temperature in terms of the physical and chemical properties of the propellant.



### III. PROPELLANT IGNITION IN THE SHOCK TUBE

#### Introduction.

Several previous reports and publications [6][7][8] have discussed the ignition of propellant samples when subjected to high convective heat fluxes from hot gases generated in a shock tube. In the previously reported work [6], a 1 7/8-inch i.d. tube with a 52-foot driver section and 11-foot driven section was used to generate hot, high-pressure gases which were passed through a 1/4-inch converging nozzle, past the surface of a propellant sample and then to the atmosphere through a small orifice. Testing times up to 60 msec were realized, and ignition times from 3-45 msec were observed. Because of shock wave attenuation in this small diameter tube, the pressure pulse at the sample position was not of an ideal form; and the pressure at the sample position increases 20-30 per cent in the first 2-3 msec after the shock wave reflected. It appeared that ignition times of 3-5 msec could not be treated in the same fashion as for longer times. In order to extend the experiments to shorter ignition times, a 4-inch i.d. tube was used in later tests. Also, a comparison of ignition data in the two tubes gave an opportunity to detect any errors in the data which might be the result of apparatus characteristics. Heat transfer tests were made with this tube, and a discussion and the results of these tests are given in Appendix A. The propellant ignition results are discussed below. A detailed discussion of the work is contained in reference [13].

#### Apparatus and Procedure.

Figure 6 is a schematic sketch of the 4-inch i.d. shock tube installation. The driver section was 15.5-feet long; the driven section was 26-feet long. Mixtures of helium and air at 150-350 psia were used as driver gases to produce shock waves in air, nitrogen and oxygen. The matched interface technique was used when producing shock waves of Mach numbers from 2.0 to 4.0. The propellant samples were mounted in the triangular test section shown in Figure 7. This test section was mounted in the end of the shock tube driven section opposite the diaphragm



EQUILATERAL TRIANGULAR  
HOLE 0.673" SIDES

0.5" DIAMETER  
QUARTZ WINDOWS

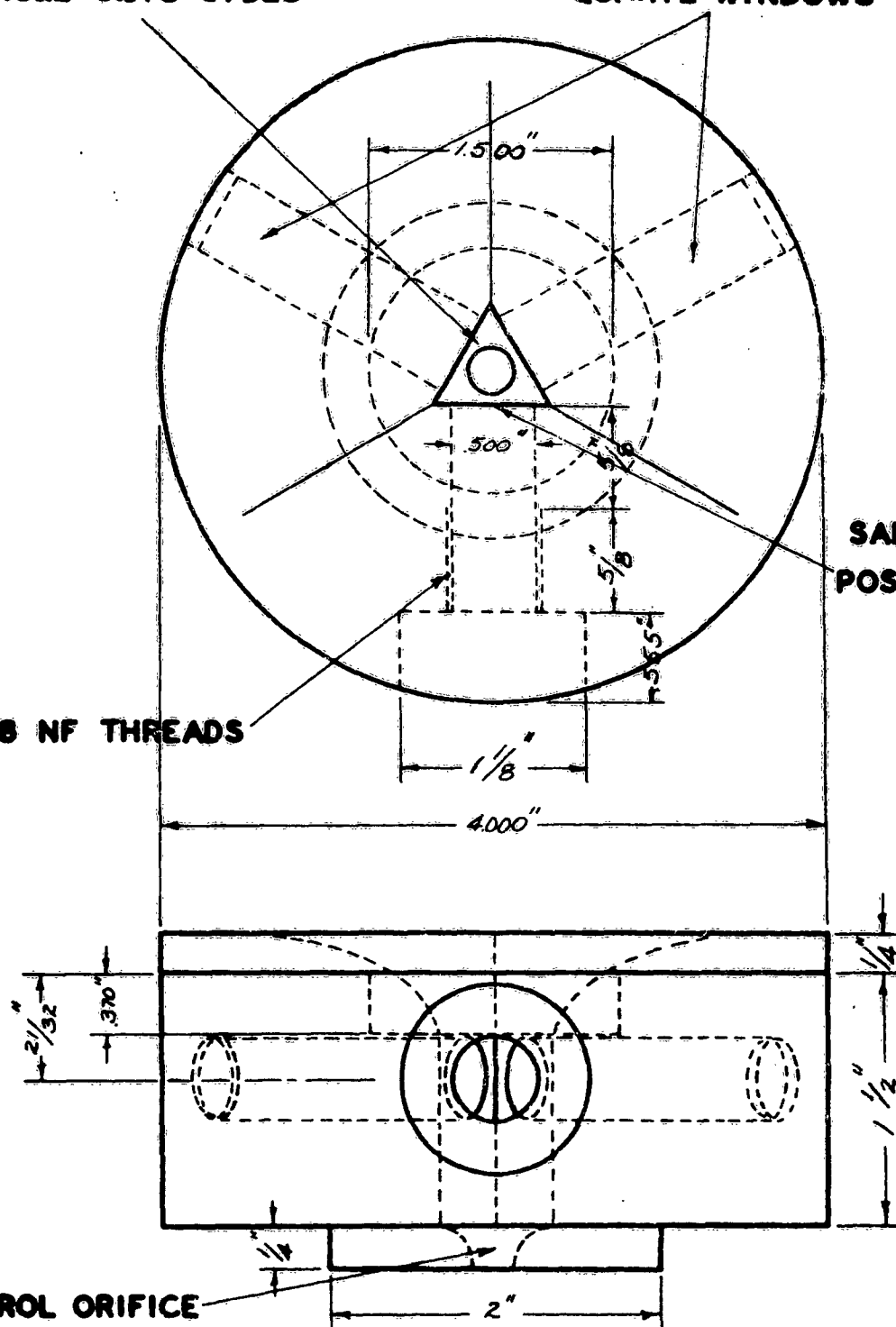
9"-18 NF THREADS

SAMPLE  
POSITION

CONTROL ORIFICE

TEST SECTION

Figure 7



# PROPELLANT SAMPLE HOLDER

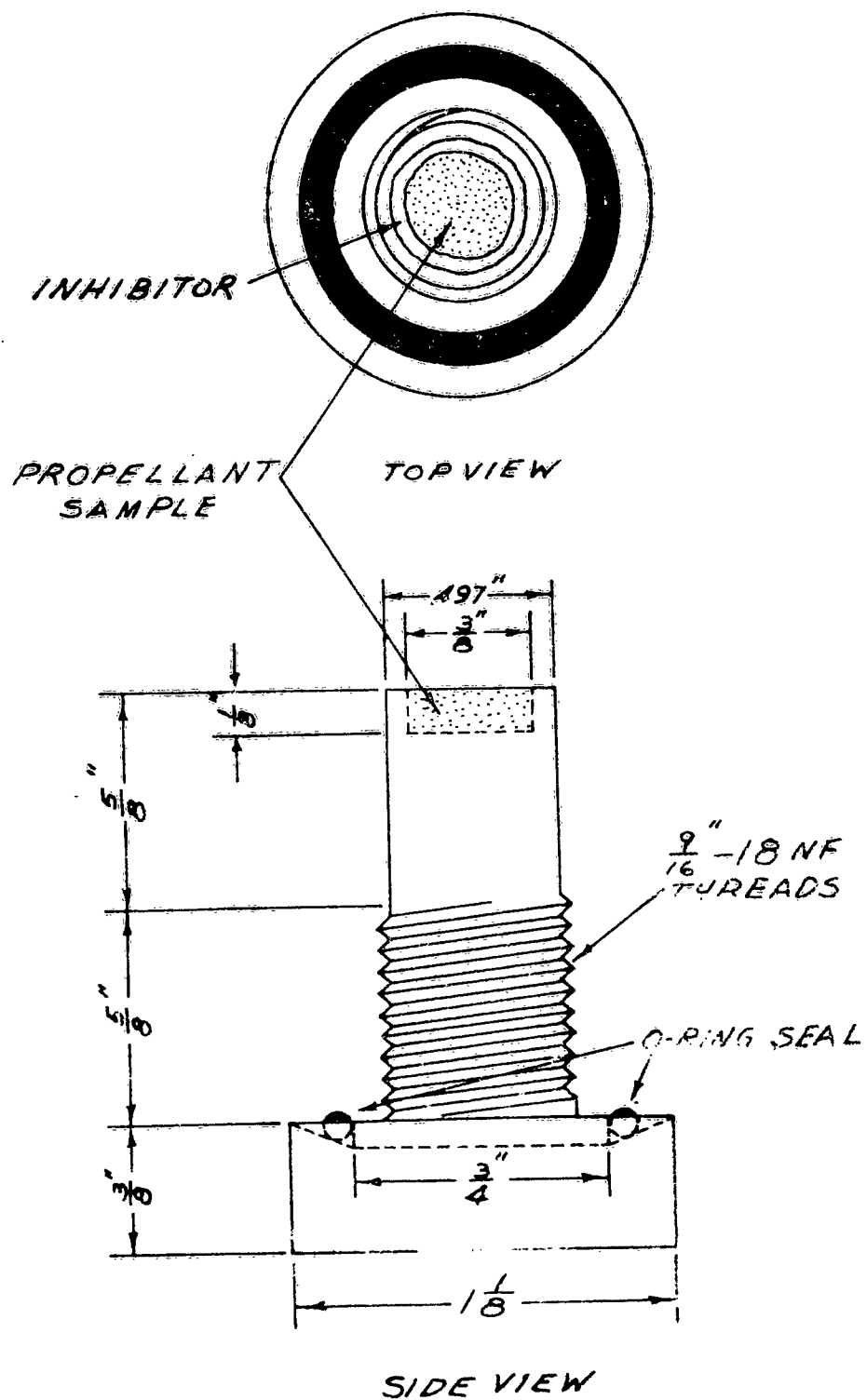


Figure 8

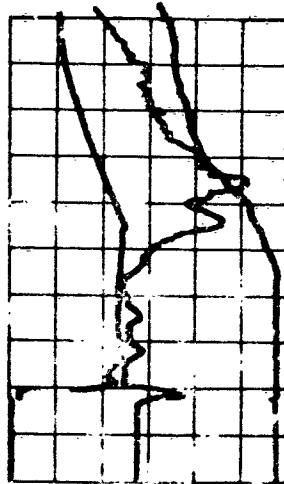
position. The propellant sample was held in the sample holder (Figure 8) with the propellant surface forming one side of the triangular duct. Quartz windows formed the other two sides of the duct. The propellant surface could be viewed by a photocell or a high-speed camera through one window. If desired, the propellant surface could be illuminated by a strong light source through the second window.

With the side of the flow control orifice (Figure 7) open to the atmosphere sealed by a small piece of tape, the pressure and gas composition in the driven section could be adjusted to any desired value. Air and helium were mixed in the driver section. The gases were introduced through a small pipe running the length of the driver section. Each gas entered the driver section through small holes drilled at 6-inch intervals in the pipe. When the desired driver gas pressure was obtained, a scribed, copper diaphragm was burst by a solenoid-driven plunger. The shock wave generated by bursting the diaphragm passed down the driven section and reflected from the end of the tube and the test section. The hot, high pressure gases generated by the shock wave passed through the triangular nozzle, flowed across the propellant surface, and then expanded to atmospheric pressure through a flow control orifice. Circular orifices of 1/4, 5/16 and 3/8 inch diameter terminated the triangular duct. The duct area was equivalent to a hole of 1/2-inch diameter.

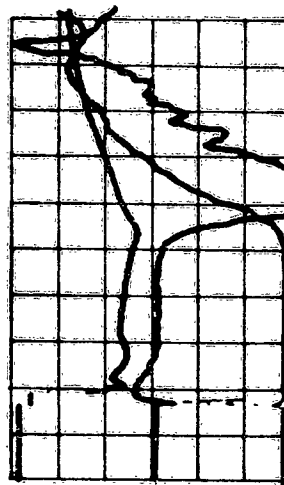
The pressure pulse at the sample position approximated the pulse form predicted from ideal shock tube theory (Figure 9), and essentially constant pressure (and gas flow rate) was maintained at the sample position for 6-12 msec. The incident shock wave velocity was measured over three 5-foot intervals in the driven section. The gas temperature behind the reflected shock wave was calculated from the wave velocity. The observed pressure measured during each run and the calculated gas temperature were suitably combined with the results of the heat transfer study to permit calculation of the heat flux to the propellant surface.

The surfaces exposed to the hot gases of all propellant samples were cut with a sharp razor blade just prior to a run. Thus, surface aging effects were eliminated. The tests were made with the samples at room

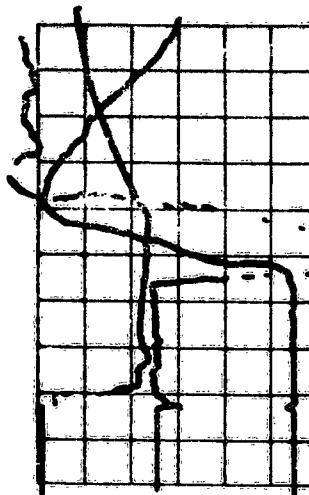
# IGNITION-TEST OSCILLOSCOPE TRACES



709 - 3  
 $M = 3.60$   
 $P_0 = 156$  psia  
 $1/4''$  orifice



709 - 2  
 $M = 3.59$   
 $P = 160$  psia  
 $5/16''$  orifice



629 - 1  
 $M = 3.52$   
 $P = 144$  psia  
 $3/8''$  orifice

C propellant in air  
 Top trace is pressure (-50 psi./div.)  
 Bottom trace is light signal  
 Middle trace is inverse of light signal derivative  
 Sweep rate is 2 msec./div. in each case

Figure 9

temperature. As indicated in Figure 8, the edge of the samples was carefully restricted to prevent gas flow between the side of the sample and the sample holder wall. An acrylic resin inhibitor was used in nitrogen and air, and an inorganic copper oxide-phosphoric acid cement inhibitor was used in oxygen. A description of the propellants used in this study is given in Table II.

### Results.

The results of this ignition study are summarized in Tables IX-XVI and in Figures 10-15. In these tests, the ignition time ( $\theta_1$ ) was defined as the interval between the arrival of the shock wave at the sample position and the first indication of a light signal from the propellant surface. Typical oscilloscope traces are shown in Figure 9. The brief signal seen coincident with the shock arrival apparently was the result of atmospheric dust and was neglected. Figures 10-15 are logarithmic plots of the square root of the ignition time versus a calculated surface heat flux. For tests in air and nitrogen, in which the surface was heated almost exclusively by convective heat transfer, the surface heat flux was taken to be that constant flux which would heat the propellant to the linearly estimated ignition temperature in the observed ignition time. In the tests in the 1 7/8-inch tube, when oxygen was used in the driven section, it appeared that the convective heating was supplemented by the effects of chemical reaction. For these oxygen tests, the surface flux was taken to be equal to the product of the surface heat transfer coefficient and a mean temperature difference between the gas and solid surface temperature and the initial propellant temperature. This calculated flux made possible the presentation of air, nitrogen and oxygen data in one plot. Only qualitative results can be inferred from such a plot for the ignition results in oxygen. For oxygen tests in the 4-inch tube, the data have been plotted in the same fashion. If no reaction occurs between the oxygen and the propellant, both techniques for calculating the surface heat flux give essentially the same value for the flux.

In all cases, the data from the 4-inch tube are compared to the results from the 1 7/8-inch tube. In Figures 10-15, data labeled "Baer" were obtained in the 1 7/8-inch tube; all other data are from the 4-inch tube. Because the duct area at the sample position for the 4-inch tube

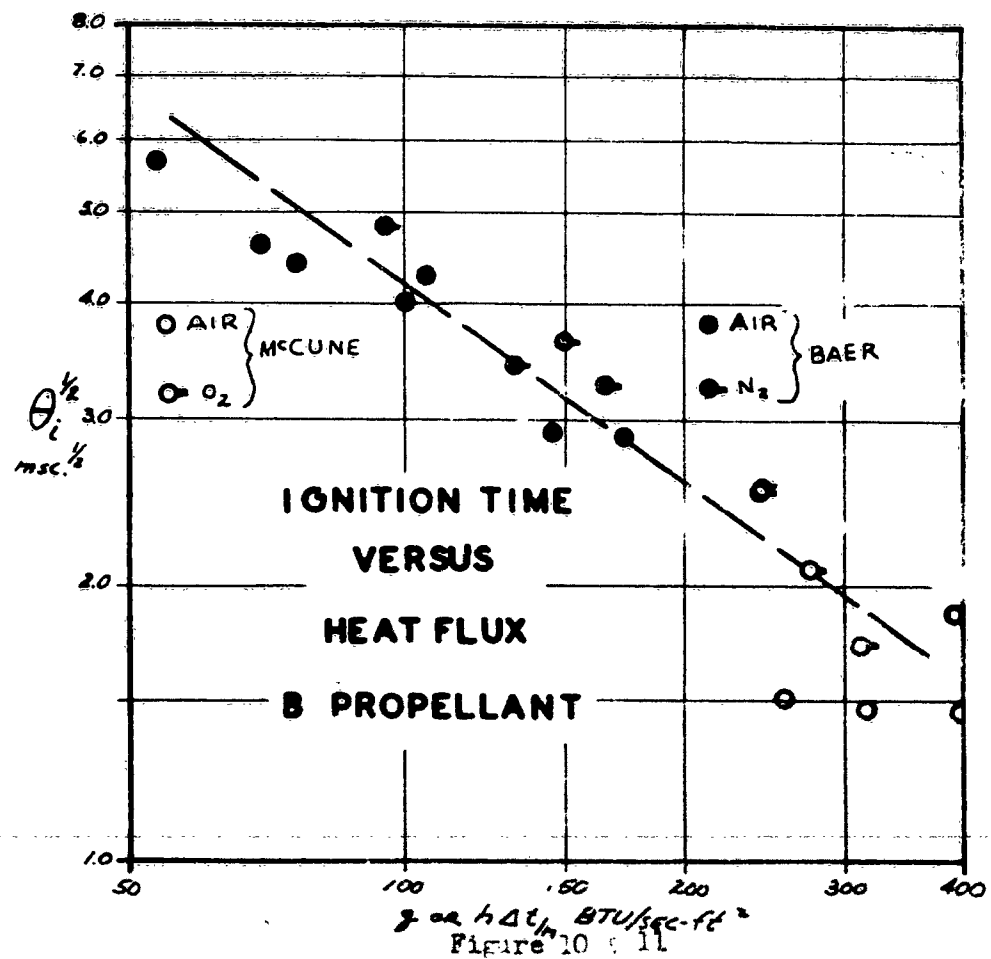
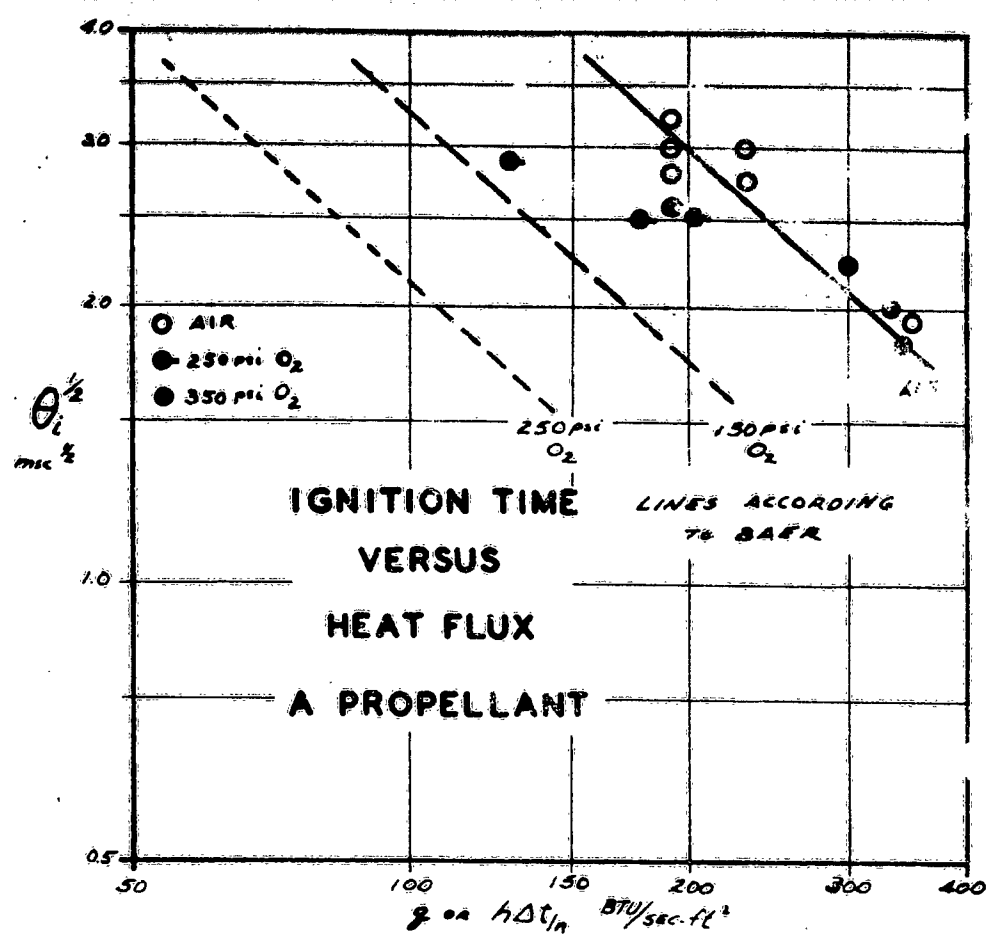


Figure 10 & 11



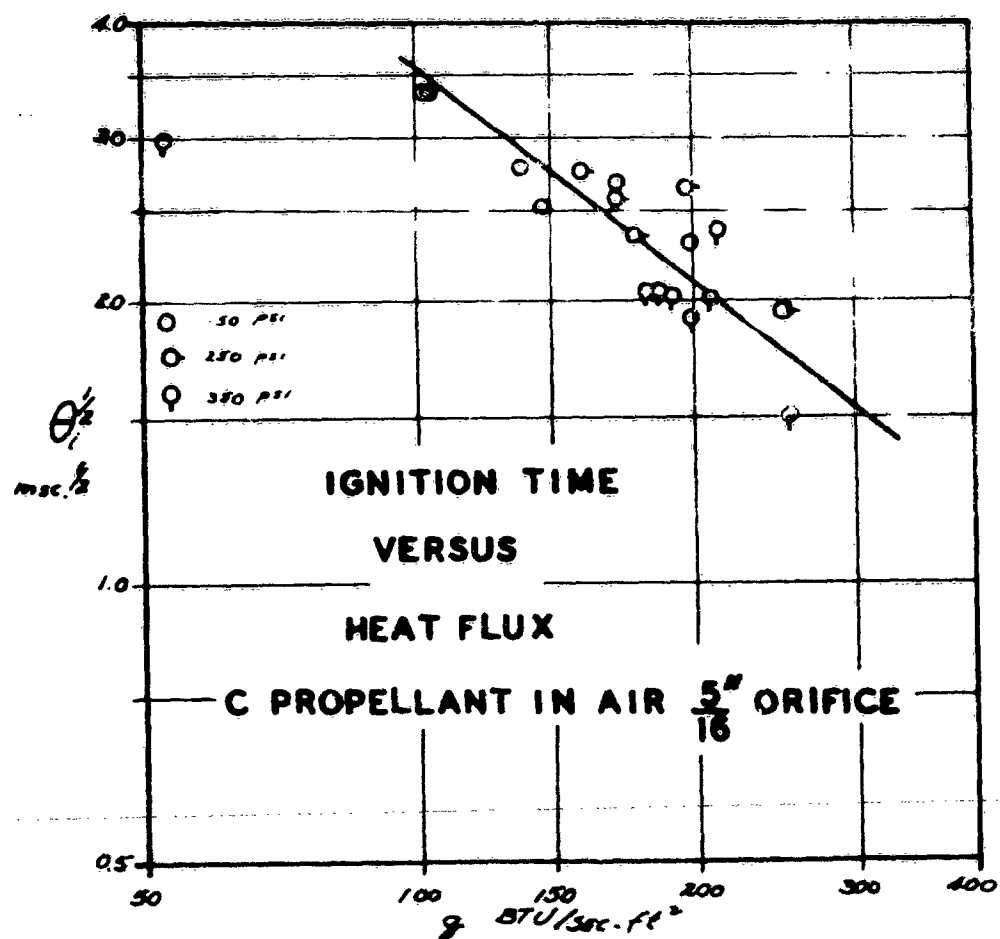
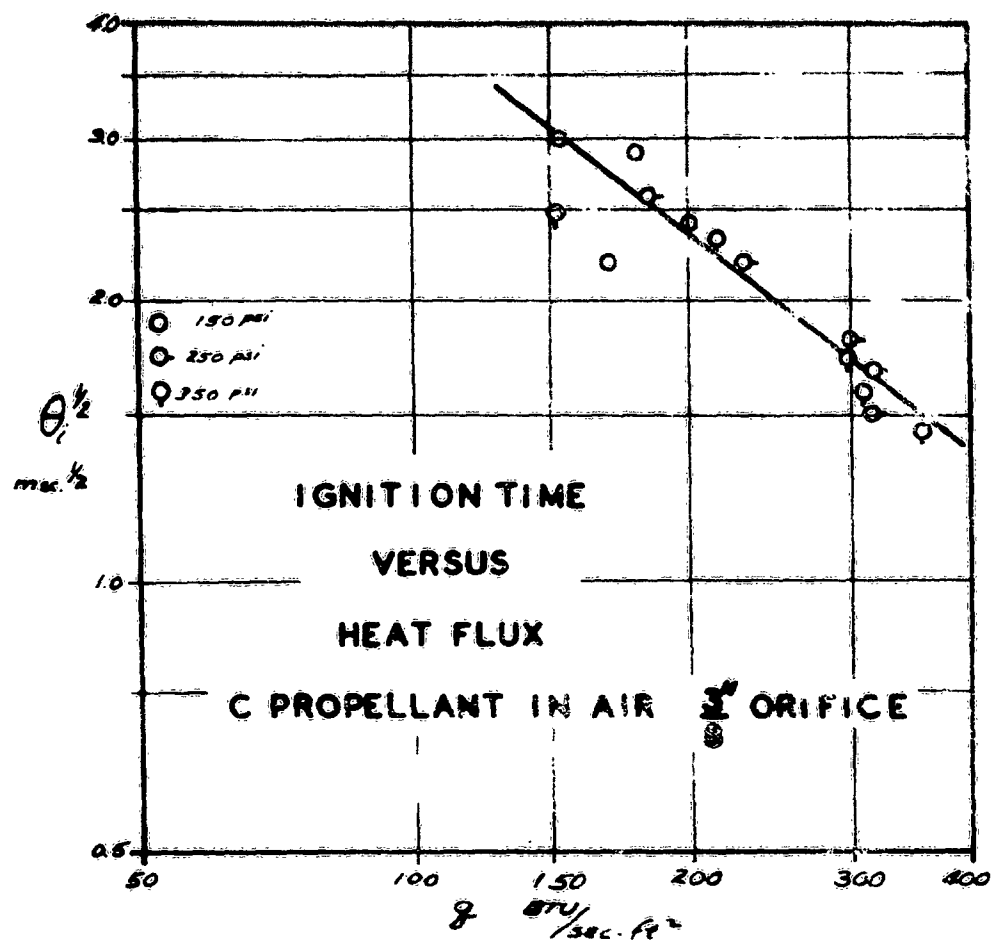


Figure 12 & 13

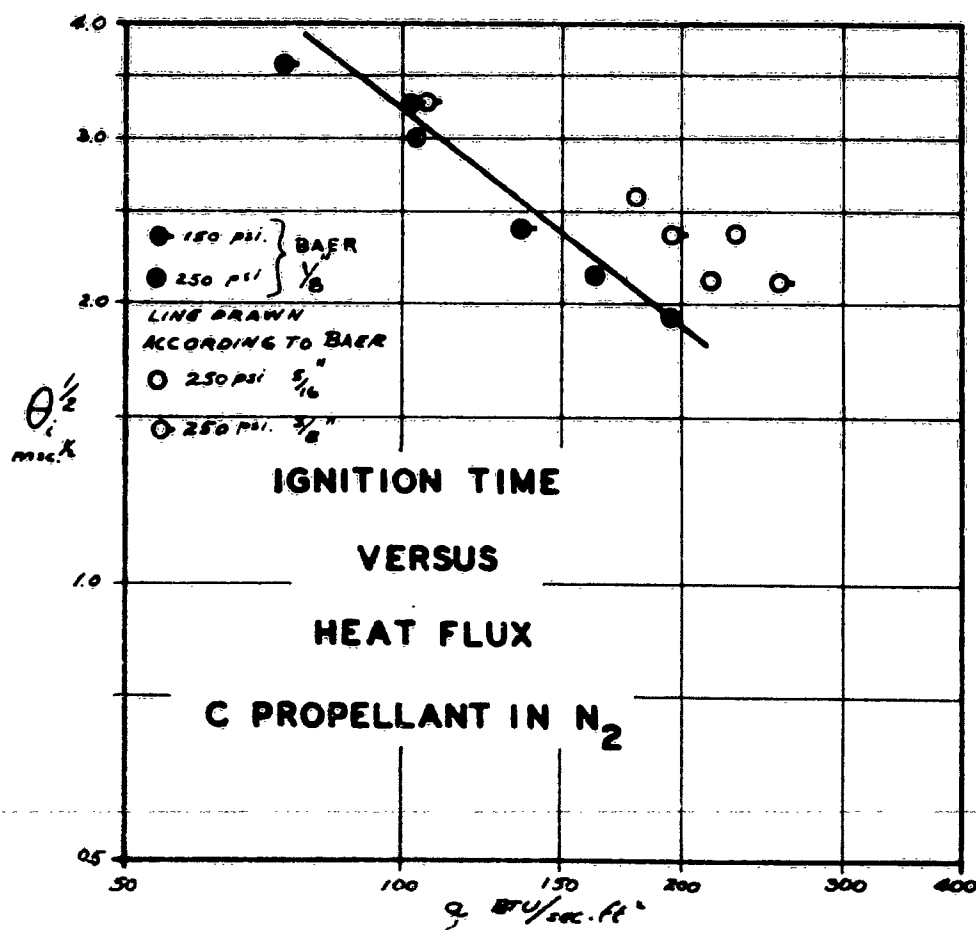
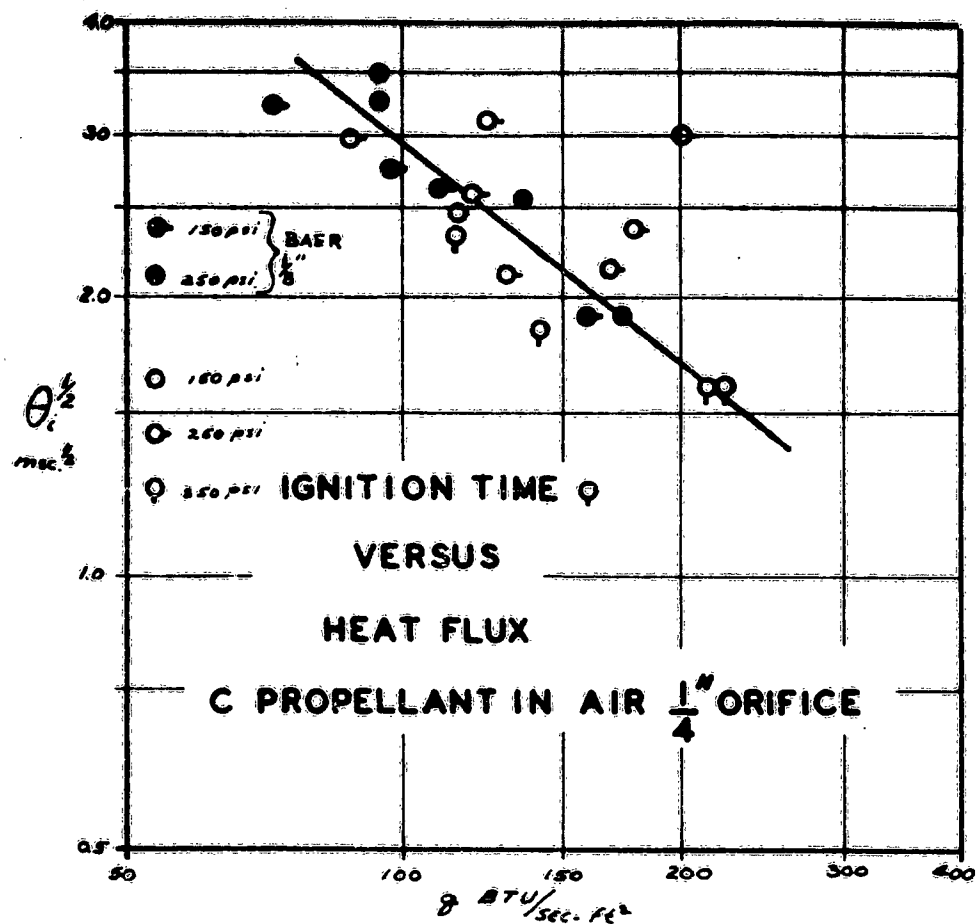


Figure 14 & 15

and the 1 7/8-inch tube were in the ratio 2:1, data from the 4-inch tube in which a 1/4-inch orifice was used are directly comparable to results from the 1 7/8-inch tube with the 1/8-inch orifice. To obtain ignition in the shorter test times available in the 4-inch tube, higher fluxes were required. These fluxes were obtained by using larger (5/16, 3/8) flow control orifices.

The data for A propellant ignition is summarized in Figure 10. The results for ignition in air are in very good agreement with the results from the 1 7/8-inch tube. For ignition in oxygen, the results in the 4-inch tube indicate that (for the large orifices at least) the oxygen does not strongly affect the ignition, and essentially the same ignition times were obtained in air as in oxygen. In the previous tests, oxygen in the gas phase was found to reduce significantly the ignition time. It appears that the higher gas velocities associated with the larger flow control orifices produced surface disturbances which interfered with the oxygen-fuel reaction.

Ignition of the B propellant was obtained only under special conditions and in most cases, the burning was stopped by the rarefaction wave. Figure 1 shows the results of tests obtained in air and oxygen in the 4-inch tube. Again the results are in agreement with those from the previous work. The oxygen appears to produce little or no effect on the ignition when the large orifices were used.

Ignition tests on the C propellant in the 4-inch tube were somewhat more extensive than for the other propellants. In the previous work in the small shock tube, the C propellant was found to be easily ignited, and a further study at shorter ignition times was indicated. The results of tests in the 4-inch tube are shown in Figures 12, 13, 14, and 15. Some effect of the orifice size was detected in these tests. The high velocity of the gas flowing past the propellant apparently had an adverse effect on the ignition process. Figure 14 shows results of tests from both shock tube studies; and indicates that with comparable orifices, the ignition results were similar. The comparison shown in Figure 15 for runs in nitrogen shows poor agreement between the tests in the two shock tubes. Since only the large orifices were used in these nitrogen tests in the 4-inch tube, it appears that the adverse effect of the high gas velocity at the propellant surface produced this difference.

### Conclusions.

1. For the same conditions of gas pressure temperature and velocity at the propellant position, the ignition times observed in the 4-inch tube were in very good agreement with the results previously reported for tests in the 1 7/8-inch tube. This shock tube ignition technique thus appears to yield results that are not characteristic of a single apparatus.

2. Since the gas velocity at the throat of the flow control orifices is sonic, high gas velocities are obtained at the sample surface as the ratio between the duct area at the sample to the orifice area approaches one. With ratios less than 4:1, an effect of the gas velocity was noted. The ignition times for the C propellant appear to be functions of this ratio and the effect of oxygen in the gas phase on the ignition process appeared to decrease as this ratio approaches one.

3. Because of the complications introduced when the ignition time is a function of the gas velocity as well as the surface heat flux, the most easily analyzed data were obtained with high duct area to orifice area ratios. In practical operation, this condition restricts the maximum heat fluxes available to the values which give ignition times greater than about 5 msec. As a consequence of this restriction, the 4-inch tube possesses no advantages over the 1 7/8-inch tube for ignition studies.

4. The unusual ease of ignition at high fluxes of the C propellant was again demonstrated, but the reasons for this characteristic are still not completely understood. The unusually fine particle size of the ammonium perchlorate in this propellant is probably linked to its ease of ignition.

#### IV. EXPLORATORY STUDIES

##### Diffusion Flame Experiments.

A widely held belief with regard to the combustion of solid propellants is that the strongly exothermic reactions occur in the gas phase between the vaporized decomposition products of propellant ingredients. It is to be expected that valuable information about the burning process can be obtained if the gaseous reactants are generated separately, then brought together for reaction. The technique used in an attempt to do this employed a diffusion flame between a large body of pressed ammonium perchlorate and a large body of binder-fuel--the phenomenon described as a "chemical arc." Energy feedback from the flame zone decomposed the fuel and the oxidant, thus supplying reactants.

The oxidizer bodies, pressed at about  $10^5$  psi. to greater than 99 per cent theoretical density were disks, 0.25, 0.5 or 1 inch in diameter and about 1/4-inch thick. Fuel bodies were of comparable size. Ignition was achieved with a hot wire pressed between the two bodies. When the flame was established, the bodies were separated. When the fuel was butadiene-MVP rubber, the flame was stable for separations up to about 3/8 inch, pressure being atmospheric. The process was studied visually and with the help of high-speed cinematography.

Mechanical difficulties arising from cracking and spalling of the perchlorate pellets under thermal stress and difficulty in controlling the geometry of the burning system frustrated the taking of quantitative data. The experiments were therefore discontinued after about 100 tests.

Some interesting qualitative information was obtained. The light intensity of the flame, and the regression rates of both substances increased markedly as the separation distance was reduced, probably due largely to the more concentrated energy release and more effective energy feedback, also to the decrease in heat losses as the separation decreased. The luminous part of the flame was definitely in the gas phase, away from the ammonium perchlorate surface.

During many of the runs, small whiskers were seen, apparently growing from the perchlorate face. They were most numerous and large

near the edges of the oxidizer pellet, smaller and sometimes absent near the center of the surface. As observed in the Fastax shots, they grow to full size rapidly, in less than 1 to 2 milliseconds, then lose and grow new branches during their life span, which ranges from a few milliseconds to several seconds. These whiskers remain on the surface after the flame is quenched. Observed under a microscope, they are lacy dendritic structures of about .005 to .01 inch in longest dimension, with a few reaching lengths of up to .05 inch. Their configuration is stable; they do not change appreciably in several days.

Chemically, it has been established only that they are not ammonium chloride. The present interpretation is that the ammonium perchlorate sublimates from the surface, which consists of superheated material in the normal, low-temperature orthorhombic form, then condenses on surface irregularities in the more stable, high temperature cubic form. If this is so, then the surface temperature is established as being greater than the phase transition temperature (240 deg. C.) but less than the normal sublimation temperature of the cubic form. No X-ray analysis for crystal form has been attempted, it being presumed that reversion to the orthorhombic form would occur before the analysis could be performed.

#### Effect of Pressure Changes on Burning Propellant.

The steady burning of a solid propellant is a complex sequence of interrelated and coupled processes. There is no reason to expect—indeed, one would not expect—that empirical and quasi-theoretical descriptions of it will apply also to transient burning. In particular, the familiar equations relating burning rate to pressure are expected to fail if the time characteristic of the pressure change, as measured perhaps by  $\left| p(dp/dt)^{-1} \right|$ , is not much greater than the relaxation time associated with establishment of a new steady state. This failure is suspected in the study of the ignition transient, thrust termination, and such irregular combustion processes as oscillatory burning and chuffing.

The relaxation times for combustion are, therefore, of considerable interest, and quantitative information is scarce. The logical attack on the problem of providing the information is to observe the response of burning propellant to suddenly-applied pressure changes. On the

intuitive supposition that relaxation times are of the order of 1 to 10 msec., the investigators in the project have considered that controlled shock waves (characteristic time less than one microsecond) and strong rarefactions (order of 0.1 to 10 msec.) may be used.

One-half-inch strands were mounted in the driven section of a 4-inch shock tube and ignited on the end facing the approaching shock wave. The end plate of the driven section was left off, so that burning took place at atmospheric pressure and the shock wave was not reflected. The burning surface was observed by means of high speed photography through a window in the tube wall. In the few experiments performed, it was observed that the propellant was extinguished before arrival of the rarefaction, presumably by the high-velocity (about 900 ft. per sec.) gas following the Mach 1.5 shock waves. The results, considered of no general value, are not reported in detail. Future work will employ samples mounted in the driven and end-plate, also higher pressures and weaker shock waves.

The rarefaction work was somewhat more extensive, and is proceeding on the basis of theoretical considerations investigated during the period of this contract. Because the theory of the operation of a rarefaction tube is not widely known, though the underlying principles have long been understood, the theory is presented in some detail in Appendix B.

A rarefaction or expansion wave can be produced in a pressurized tube when a diaphragm is burst at one end. The pressure ratio across the rarefaction can be varied by changing the properties of the gas in the tube and by installing nozzles of different areas at the tube outlet. The wave diagram in Appendix B illustrates the movement of the head and foot of the rarefaction after the diaphragm is burst. The gas in the tube is initially at  $P_0$ . The head of the rarefaction moves into the undisturbed gas at the velocity of sound in that zone. The foot follows the head at a lower velocity, with the result that the wave becomes wider as it moves into the tube. The pressure after the passage of the rarefaction is  $P_1$ . The head and foot of the rarefaction reflect off the closed end of the tube. With the passage of this second rarefaction the pressure becomes  $P_2$ . Each of the zones, 0, 1, and 2, is (ideally) at a uniform state and velocity. The gas in zones 0 and 2 is stagnant; the gas in zone 1 is moving toward the nozzle outlet.

Propellant strands 1/2-inch in diameter and 2- to 4-inches long were mounted in the closed end of a 4-inch diameter rarefaction tube. In most tests the end of the sample was cut at about a 45 degree angle so that the burning surface was visible through a 1-1/2-inch diameter window in the side of the tube. Nitrogen gas was used to pressurize the tube to prevent gas phase reactions with the propellant ignition products. Nozzles giving pressure drops of 30 to 74 per cent (i.e.  $p_2/p_0$  from 0.7 to 0.26) were used.

The results in Table XVII were obtained from measurements of light intensity by means of a photocell and from observations of the burning surface using high-speed photography. It will be observed first that the propellants burning with greatest stability are those observed, in the ignition study, to be most easily ignited. The results at hand suggest that it is the fractional change in pressure (or rate of change of log pressure) that determines whether the flame is stable. This tentative conclusion is compatible with the premise that for stability, the relaxation time of the combustion process must not be much greater than the characteristic time of the rarefaction,  $p(dp/dt)^{-1}$ . Ciepluch [9] assumes that the time rate of pressure drop,  $dp/dt$ , is the decisive variable.

It was mentioned in Table XVII that a flash of light was seen during runs with C propellant. The intensity of the light signal was at times higher after the first rarefaction than before its passage. A flash of light was also seen in the high speed motion pictures. With the arrival of the rarefaction the flame was pulled away from the surface. After the rarefaction had passed the flame flashed back to the surface with an intense light signal. The two aluminized propellants did not show this effect. It is speculated that the presence of aluminum accounts for the difference.

#### Flame Spread.

The role of flame spread in the overall ignition process has been briefly investigated with the composite propellants. Slabs of propellant two inches long, one-half to three-quarters inch wide, and of thicknesses from one-sixteenth to one-half inch were cemented to an inert base. The edges were lightly restricted; the top faces were freshly cut surfaces. The slabs were ignited at one of the short ends. The following observations were made for burning at atmospheric pressure:



- (1) With the thinner slabs (to one-eighth inch), burning occurred on a flat surface forming an angle of approximately 45 degrees with the unburned top surface. The rate of flame spread, the speed with which the flame edge progresses along the unburned top surface, is the normal burning rate times the secant of this angle, or about 1.4 times the normal burning rate.
- (2) Thicker slabs (one-fourth inch to one-half inch) were ignited near the base of the vertical edge. The flame spread to the top surface, where it established the canted burning surface observed on thin slabs. The canted burning surface grows at the expense of the original vertical burning surface until the latter disappears. While both burning surfaces are present, the two corresponding jets of hot gasses and particles are quite distinct.
- (3) The same behavior was observed for slabs cemented to a thin sheet of copper instead of an insulating material.
- (4) A blast of air opposing the advancing flame on the top surface prevents the formation of the canted burning surface.

One-eighth inch slabs were similarly burned in a window bomb at 250 psi. The canted burning surface was again observed, again at an angle of about 45 degrees to the unburned surface. The normal burning rate and the rate of flame spread appear to have the same pressure dependence.

This study has yielded an interesting by-product in the observation that there are two modes of aluminum behavior at the burning surface. In propellant A, containing only two per cent aluminum, most of the aluminum particles appear to explode on the surface. In propellant E, containing 12 per cent aluminum, the particles are blown away from the surface.

The bright color of the aluminum particles on the surface testified that the temperature of the aluminum is much higher than that of the rest of the surface. The hot particles, whether exploding at the surface or being blown off, provide a continuous source of ignition, and thus tend to stabilize the flame position. The combustion process is therefore less able to couple with the amplify pressure fluctuations than when aluminum is absent. This is offered as a partial explanation of the effectiveness of aluminum in supressing severe oscillatory burning.

The results of the flame spread work suggest that flame spread is too slow to contribute significantly to the ignition process. The rapid growth of the burning zone when large surfaces are ignited in rocket practice does not proceed by the mechanism of flame encroachment on new surface from adjacent burning surfaces. It is, for the most part, simply delayed ignition by externally supplied heat flux, part (or in extreme cases all) of which is provided by other propellant ignited earlier.

## APPENDIX A

### HEAT TRANSFER

For analysis of ignition data from the shock tube tests, it was necessary to have some knowledge of the heat transferred to the propellant surface. Heat-transfer rates for the transient heating by convective heat transfer in the shock tube were obtained in an independent study. Heat fluxes were calculated from temperature-time traces obtained from heat-flux gages mounted at the propellant position in the test section. The heat-transfer rates to these gages were translated to equivalent heat transfer to the propellant from knowledge of the thermal properties of gages and propellants. In the course of this work three independent heat-transfer studies were conducted since three different test sections were used with two different shock tubes.

Heat-flux gages for these tests were prepared by painting and firing a thin film of liquid Bright Platinum No. 05-x manufactured by Hanovia Chemical and Manufacturing Company on substrates of glass, soapstone, pyroceram, and alumina. This procedure produced a thin platinum film 0.1 to 1 micron thick on the surface of the substrate. The thermal responsivity,  $\Gamma$ , of the substrate and temperature coefficient of the platinum film of the gages were measured. The surface temperatures of the substrate are measured by the thin-film, platinum resistance thermometer. For short-time intervals, the theory of heat conduction to a semi-infinite solid may be applied and surface temperature-time data used to obtain heat flux at the gage surface. With an appropriate recording circuit, very accurate temperature-time relationships can be obtained for the 50-60 millisecond test time. Details of the gage construction and theory and of the electrical circuitry can be found in references [2], [5], [10], and [13].

During tests in the shock tube, the surface temperature at the heat-flux gage increased discontinuously as the incident shock reflected from the end of the test section. The temperature then increased continuously until the first rarefaction wave arrived at the test section. At high Mach numbers, the diffuse interface was sufficiently close to the end of the shock tube to allow some of the cold driver gas to mix with the processed gas and enter the test section 15 to 20 milliseconds after the start of the test. This effect influenced heat transfer in the test section before the rarefaction wave arrived.

The magnitude of the initial, discontinuous temperature jump was a function of the incident shock Mach number and pressure behind the reflected shock for the conditions employed. This relationship was determined experimentally and results are shown graphically in Figure A-1. The results tabulated in Tables XX and shown by Figure A-1 are for different test sections with bell-mouthed entrances. These sections were: (1) a circular cross-section with a plastic entry nozzle, used at the end of the 1 7/8-inch diameter shock tube; (2) a triangular cross-section with a fired soapstone bell-mouthed entry, used at the end of the 4-inch diameter shock tube; and (3) a rectangular cross-section with a steel entry nozzle, used at the end of the 1 7/8-inch diameter shock tube. The gas flow in each test section was controlled by a critical flow orifice downstream from the test section. Figure 7 shows the triangular section. Experimental results for the 1 7/8-inch and 4-inch diameter shock tube with glass and soapstone inlet sections show good agreement, except for large Mach numbers. Recent results with the third test section and the 1 7/8-inch shock tube gave lower values of the initial temperature rise for all Mach numbers. This discrepancy is assumed to be the result of energy loss to the steel entry nozzle. Complete data obtained with Section No. 1 are given in references [5] and [6].

In tests in the 1 7/8-inch shock tube it was found that after the initial temperature rise, the increase with time of the surface temperature of the gage fit the relationship for the surface temperature of a semi-infinite solid heated from a constant temperature source through a constant surface heat transfer coefficient:

$$\frac{T_s - T_j}{T_g - T_j} = 1 - e^{N^2} \operatorname{erfc} N \quad (A1)$$

$$N = \frac{h \theta^{1/2}}{\sqrt{\rho c}} \quad (A2)$$

where  $T_s$ ,  $T_g$ , and  $T_j$  are temperatures at the gage surface, gas temperature, and jump temperature, respectively;  $h$  is the surface heat transfer coefficient.

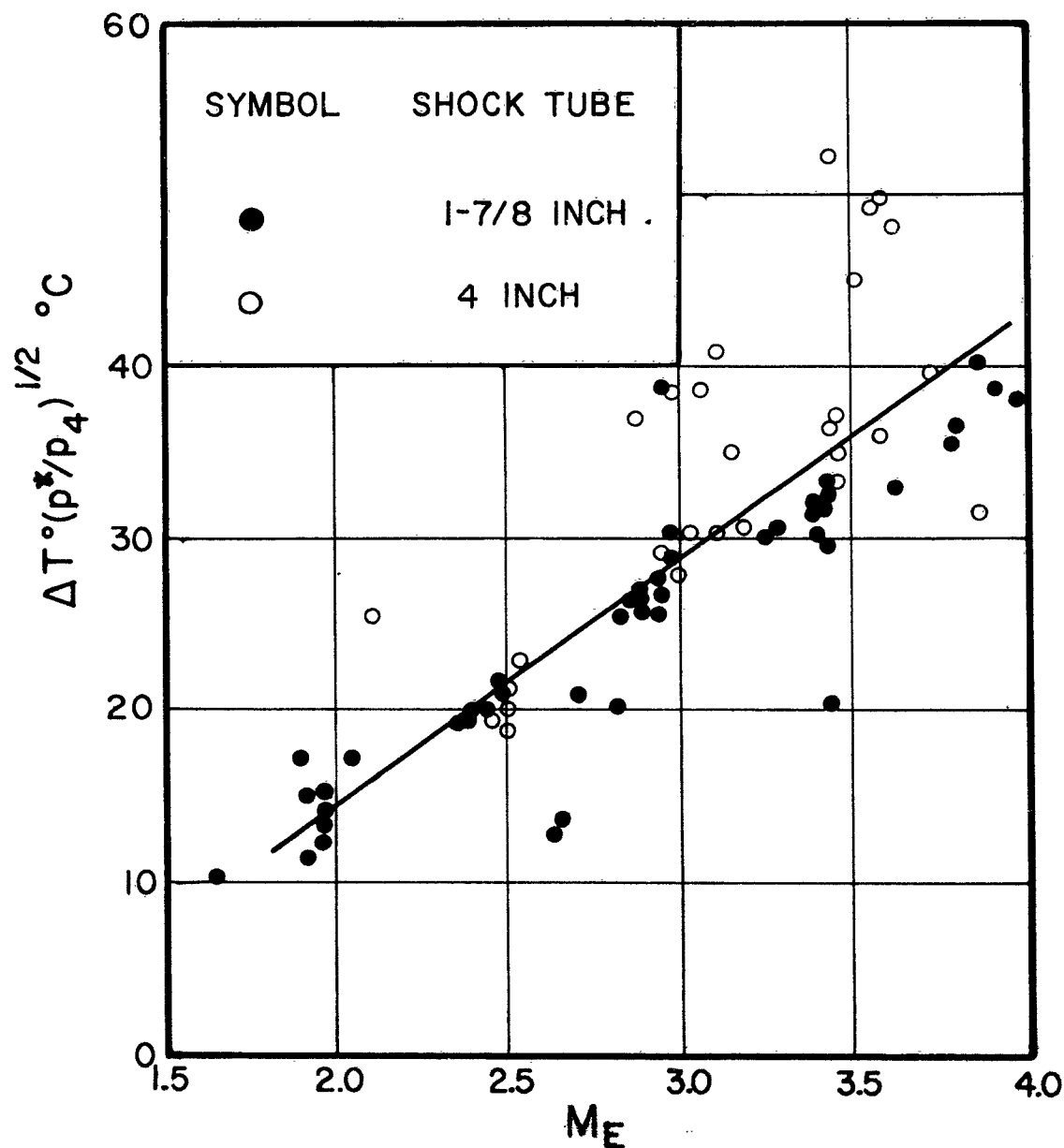


Figure A-1. Correlation of the Initial Discontinuous Surface Temperature Rise of the Heat Flux Gages with the Shock Mach Number at End of the Shock Tube. All values of temperature use have been corrected to a reference pressure of 100 psia ( $p^*$ ) and to a substrate  $T$  of  $5.52 \text{ Btu/hr}^{1/2} \text{ ft}^2 \text{ } ^\circ\text{F}$ .

The thermal responsivity of the gage,  $\Gamma$ , is the square root of the product of thermal conductivity, specific heat, and density of the gage substrate. Equation (A-1) can be derived from transient heat conduction theory if one assumes a total heat flux which is the sum of two fluxes, one proportional to the reciprocal of the square root of time and a second proportional to the solid-surface-to-gas stagnation temperature difference. The second proportionality constant is the heat transfer coefficient [5].

Although Equation (A-1) appeared to represent adequately the gage surface temperature-time relationship for 50-60 millisecond testing time in the 1 7/8-inch shock tube, a more complicated expression was needed to represent this relationship in the 8-10 millisecond testing time in the 4-inch tube. This result is given as follows:

$$\frac{T_s - T_0}{bT_g - T_0} = k \sum_{n=1}^{\infty} B^n \left[ \operatorname{erfc} 2n\phi + \operatorname{erfc} (2n+2)\phi - \frac{2T_g(b-1)}{bT_g - T_0} \operatorname{erfc} (2n+1)\phi \right] \quad (A3)$$

where  $b$  is a factor which accounts for the shock wave amplification as it passes into the converging channel,  $T_0$  is the initial gage temperature,

$$B = \frac{1 - \alpha}{1 + \alpha}, \quad k = \frac{\alpha}{\alpha + 1} \quad \text{and} \quad \phi = \frac{\Gamma'_a}{2h\theta^{1/2}}.$$

According to the theory,  $\alpha$  should be equal to the ratio of thermal response values of air to solid. Because the density of air is a function of temperature it was necessary to determine this factor experimentally. The apparent thermal response for air ( $\Gamma'_a$ ) was about twice the value calculated from the properties of air. The factor  $b$  is 1.3 to 1.4 and can be calculated from shock tube theory. A detailed discussion of Equation (A-3) is found in reference [13].

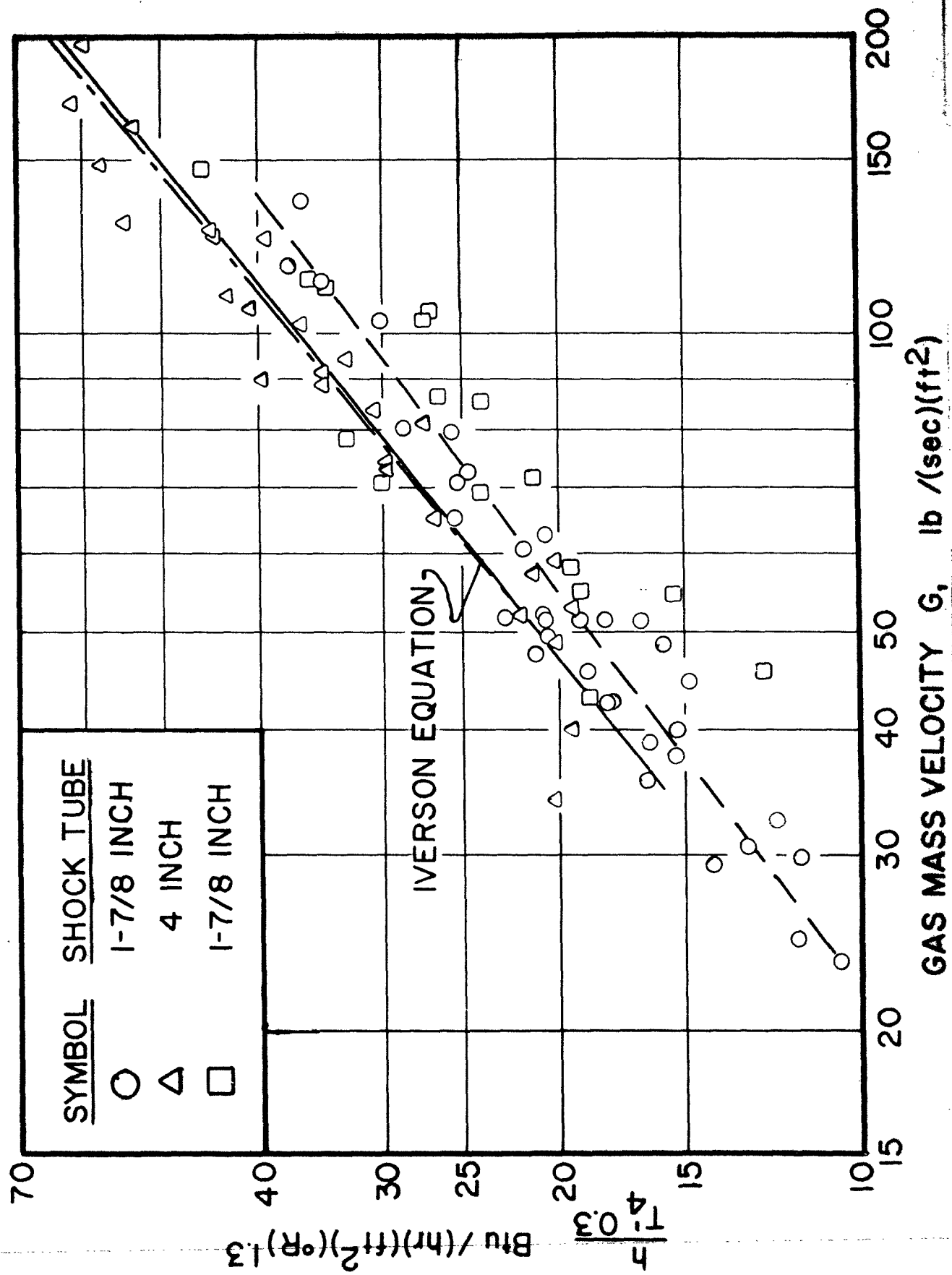


Figure A-2. Heat Transfer Coefficients to the Walls of the Various Shock-Tube Test Sections.

Heat transfer coefficients determined from all the temperature-time data are shown in Figure A-2. Data from test sections No. 2 and No. 3 are given in Tables XIX and XX. These heat transfer coefficients can be represented by an equation of the form:

$$h = a T_g^n G^m \quad (A4)$$

where  $h$  is the heat transfer coefficient,  $T_g$  is the gas stagnation temperature, and  $G$  is the gas mass velocity past the gage surface. With critical flow at the control orifices, mass velocities could be calculated from the effective orifice area and the stagnation state of the gas.

For the 1 7/8-inch diameter shock tube with either a circular or rectangular test section with a bell-mouthed inlet, heat transfer coefficients could be represented by:

$$h = 1.02 T_g^{0.3} G^{0.75} \quad (A5)$$

for  $h$  in Btu/(hr)(ft<sup>2</sup>)(°F);  $T_g$  in °R and  $G$  in lb/(sec ft<sup>2</sup>)

Iverson, et al., [11] in an approximation to the Latzuko solution for steady-state point heat transfer in a circular duct following a bell-mouthed inlet arrived at an experimentally confirmed equation in the form:

$$h = 1.07 T_g^{0.3} G^{0.78} \quad (A6)$$

in the same units. For the range of mass velocities studied, the transient coefficient calculated from the data of this study are 15 to 20 per cent less than values predicted by Equation(A-5).

Heat transfer coefficients for the triangular cross-section test section of the 4-inch diameter shock tube during the 8-10 millisecond test time were 10-15 per cent higher than observed in the 1-7/8-inch tube. These values could be represented by:

$$h = 1.09 T_g^{0.3} G^{0.76} \quad (A7)$$

In the triangular section the gas mass velocity at the surface of the gage was probably higher than the average mass velocity calculated and used in Equation (A-7). This effect presumably accounts for the higher heat transfer coefficients.



In recent studies heat-flux gages made of different substrates were used. Three substrate materials, alumina, pyroceram, and pyrex glass with thermal responses of 25.1, 5.45, and  $4.44 \text{ Btu}/(\text{hr})^{\frac{1}{2}}(\text{ft}^2)(^{\circ}\text{F})$  respectively were used in these tests. Essentially the same values for the heat-transfer coefficient and the initial temperature rise (corrected for the  $\Gamma$  value) were obtained for all gages. These results confirmed earlier assumptions that surface temperatures of propellants with  $\Gamma$ 's of about  $2.5 \text{ Btu}/\text{ft}^2(\text{hr})^{\frac{1}{2}}$   $^{\circ}\text{F}$  could be calculated directly from transient heat-transfer results.

## APPENDIX B

### RAREFACTION TUBE THEORY

Below is developed an approximate "centered wave" theory of the rarefaction tube. Predictions based on it are compared to those based on less convenient exact theory and to the results of tests made in a one-inch tube. Symbols, in general different from those used in the rest of the report, will be defined as they are introduced.

The rarefaction tube as employed in the work at the University of Utah is a cylindrical tube of length  $L$ , cross-sectional area  $A_0$ , closed at one end and terminated at the other by a rounded nozzle, throat area  $A_m$ . The function of the nozzle is to control the flow rate. The nozzle is closed with a diaphragm which, when the tube contents have been brought to the desired pressure, is ruptured. The history of occurrences in the tube after diaphragm rupture is shown on the wave diagram, Figure B-1. Distance measured from the nozzle is  $x$  or  $\xi = x/L$  in reduced form and time from diaphragm burst is  $t$  or  $\tau = \frac{a_0 t}{L}$  in reduced form,  $a_0$  being the speed of sound in the undisturbed gas.

The objective of the theoretical development would be, ideally, to describe occurrences near the sample position, closed end, in terms of the controlled parameters,  $A_m/A_0$ ; the initial temperature and pressure of the undisturbed gas,  $p_0$  and  $T_0$ ; and the properties of the gas as represented by the isentropic constant,  $\gamma$ ,

$$\gamma = \left( \frac{\partial \ln p}{\partial \ln \rho} \right)_s$$

where  $p$  is pressure,  $\rho$  is density. It turns out, however, that it is more convenient to use  $a_0$  in place of  $T_0$ ,  $n$  in place of  $\gamma$ , where

$$n = \frac{\gamma + 1}{\gamma - 1}$$

and  $\sigma_1$ , which is  $a_1/a_0$ ,  $a_1$  being the speed of sound of the gas in Zone 1. Numerical subscripts refer to zones shown on the wave diagram.



$A_m/A_o$  in Terms of  $n, \sigma_1$ .

The following assumptions will be made:

1. The gas flow is one-dimensional and non-viscous.
2. The gas behaves as an ideal gas with constant heat capacity.
3. All gas expansion is isentropic.
4. The gas velocity at the nozzle throat is sonic.
5. The incident rarefaction wave is a centered wave.

The first assumption is the least sound, being worse for stronger rarefactions. A method to account for the effects of friction is described briefly later. The fourth assumption can be assured if, in the experiments, ambient pressure is less than critical, referred to  $p_1$ .

The isentropic relations are

$$\sigma = \frac{a}{a_o} = \left(\frac{T}{T_o}\right)^{1/2} = \left(\frac{p}{p_o}\right)^{\frac{1}{n+1}} = \left(\frac{\rho}{\rho_o}\right)^{\frac{1}{n-1}} \quad (\text{B-1})$$

Use is made of two equations from the theory of waves and characteristics:

$$\frac{du}{dx} = \pm \frac{a}{x} \quad \frac{dx}{dt} = u \pm a \quad (\text{B-2})$$

The first, when it is noted from Equation (B-1) that,

$$\frac{d\rho}{\rho} = (n-1) \frac{da}{a}$$

integrates to

$$u - u' = \pm (n-1) a_o (\sigma - \sigma') \quad (\text{B-3})$$

where the primes indicate reference values.

If the undisturbed gas is taken as reference and gas velocity is taken as positive to the right,  $u' = u_o = c$ ,  $\sigma' = \sigma_o = 1$

$$u_1 = (n-1) a_o (1 - \sigma_1) \quad (\text{B-4})$$

The Mach number in Zone 1 is

$$M_1 = \frac{u_1}{a_1} = (n-1) \frac{1 - \sigma_1}{\sigma_1} \quad (\text{B-5})$$

Until the return of the reflected wave (at a time later than shown on Figure B-1), steady flow conditions exist at the nozzle. Continuity gives

$$\frac{A_m}{A_o} = \frac{u_i}{u_m} \frac{\rho_i}{\rho_m} \quad (\text{B-6})$$

where subscript m refers to conditions at the nozzle throat. The concept of the steady-flow isentropic stagnation condition for Zone 1 can be invoked:

$$\frac{T_{is}}{T_i} = 1 + \frac{M_i^2}{\gamma - 1} \quad (\text{B-7})$$

If Equation (B-5) is used to eliminate  $M_i$

$$\frac{T_{is}}{T_i} = 1 + (\gamma - 1) \left( \frac{1 - \sigma_i}{\sigma_i} \right)^2$$

As sonic velocity exists at the throat of the nozzle,  $M_m = 1$ , and

$$\frac{T_{is}}{T_m} = \frac{\gamma}{\gamma - 1}$$

When  $T_{is}$  is eliminated from the last two equations,

$$\frac{T_i}{T_m} = \frac{\gamma}{\gamma - 1} \left\{ 1 + (\gamma - 1) \left( \frac{1 - \sigma_i}{\sigma_i} \right)^2 \right\}^{-1} \quad (\text{B-8})$$

As flow is isentropic,

$$\frac{\rho_i}{\rho_m} = \left( \frac{T_i}{T_m} \right)^{\frac{\gamma - 1}{2}} \quad (\text{B-9})$$

Also

$$u_m = a_m = a_o \left( \frac{T_m}{T_o} \right)^{1/2} = a_o \sigma_i \left( \frac{T_m}{T_i} \right)^{1/2} \quad (\text{B-10})$$

Densities and velocities are replaced in Equation (B-6) by their equivalents from Equation (B-4, B-9, and B-10), then  $T_1/T_m$  is eliminated by means of Equation (B-8):

$$\frac{A_m}{A_o} = (n-1) \left( \frac{n}{n-1} \right)^{n/2} \frac{1-\sigma_1}{\sigma_1} \left\{ 1 + (n-1) \left( \frac{1-\sigma_1}{\sigma_1} \right)^2 \right\}^{-n/2} \quad (B-11)$$

Thus the nozzle area ratio is related to  $\sigma_1$  and  $n$ . The problem remaining is to relate the process at the closed end of the tube to these two variables. It is interesting to note in passing that for the maximum value of  $A_m/A_o = 1$ , the minimum value of  $\sigma_1$  is obtained,  $(n-1)/n$ . According to Equation (B-4), the maximum value of  $M_1$  is therefore unity.

#### The Wave Diagram.

For region bounded by lines A, B, and C, lines of constant state (and therefore of  $\sigma$ ), the wave equation (second of Equation (B-2)) is

$$\frac{dx}{dt} = u + a$$

In reduced form, after  $u$  is eliminated by Equation (B-4) (with sign change to account for direction),

$$\frac{d\xi}{d\tau} = n\sigma - (n-1)$$

which, integrated from (0,0) to  $(\xi, \tau)$  gives, with rearrangement

$$\sigma = \frac{1}{n} \frac{\xi}{\tau} + \frac{n-1}{n} \quad (B-12)$$

Line C is a characteristic with the equation

$$\frac{dx}{dt} = u - a$$

which similarly becomes

$$\frac{d\xi}{d\tau} = \frac{\xi}{\tau} \frac{n-1}{n} - 2 \frac{n-1}{n}$$

Integration gives  $\xi(\tau)$  for line C:

$$\xi = (n-1) \tau \left( \frac{n}{n-1} \tau^{-2/n} - 1 \right)$$

or, in the more useful parametric form,

$$\begin{aligned} \tau &= \sigma^{-n/2} \\ \xi &= (n-1) \sigma^{-n/2} \left( \frac{n}{n-1} \sigma - 1 \right) \end{aligned} \quad (\text{B-13})$$

Both Equation (B-12) and Equation (B-13) apply for  $1 \geq \sigma \geq \sigma_1$ . Line C terminates at  $(\xi_1, \tau_1)$ , where  $\sigma = \sigma_1$ .

The analysis to this point, rigorous within the limits imposed by the original assumption, permits determining the point  $(\xi_1, \tau_1)$  useful below. The objective is to locate the point  $(1, \tau_L)$  and determine the value of  $\sigma$  there. This gives  $\sigma(\tau)$  and, with the help of Equation (B-1),  $p(t)$  at  $\xi = 1$ . The procedure is to focus on Line D, which begins at  $(\xi_1, \tau_1)$  and terminates at  $(1, \tau_L)$ , and to treat it in the same manner as has just been used for Line C.

An additional assumption is made, namely that the reflected wave, bounded by Lines E and F, is a centered wave, radiating from  $(\xi_0, \tau_0)$ , the intersection of E and F extended. This assumption is not compatible with the original assumption that the incident wave is centered, as pointed out by Rudinger [12]. The error introduced will be discussed later.

For the reflected wave (where  $\xi < \xi_1$ ), Equation (B-3) gives, for  $\sigma_1 \geq \sigma \geq \sigma_2$

$$u = (n-1) a_0 (\sigma - \sigma_1) \quad (\text{B-14})$$

This is introduced into the second Equation (B-3), with sign change to account for direction:

$$\frac{dx}{dt} = u - a = a_0 [(n-1)(\sigma_1 - \sigma) - \sigma] \quad (\text{B-15})$$

Equation (B-14) yields  $u_1$  when  $\sigma = \sigma_1$ , and the resulting expression can be used with Equation (B-4) to eliminate  $u_1$ :

$$\sigma_2 = 2\sigma_1 - 1$$

This is put into Equation (B-15) to obtain, in reduced form

$$\frac{d\xi}{d\tau} = (n-1)(2\sigma_1 - 1) - n\sigma$$

Integration at constant  $\sigma$ ,  $\sigma_1 > \sigma > 2\sigma_1 - 1$ , gives

$$\frac{\xi - \xi_c}{\tau - \tau_c} = (n-1)(2\sigma_1 - 1) - n\sigma \quad (\text{B-16})$$

There are two special cases of interest:

$$\begin{aligned} \sigma = \sigma_1: \quad \frac{\xi_i - \xi_c}{\tau_i - \tau_c} &= (n-2)\sigma_1 - (n-1) \\ \sigma = \sigma_2 = 2\sigma_1 - 1: \quad \frac{\xi_i - \xi_c}{\tau_i - \tau_c} &= -(2\sigma_1 - 1) \end{aligned} \quad (\text{B-17})$$

For Line D, Equation (B-14), again with the sign on  $u$  changed, is used with

$$\frac{dx}{dt} = u + a$$

to give, in reduced form,

$$\frac{d\xi}{d\tau} = (n-1)(2\sigma_1 - 1) - (n-2)\sigma$$

Equation (B-16) is used to eliminate  $\sigma$ , and integration performed, the initial condition being that D originates at  $(\xi_i, \tau_i)$ :

$$\frac{\xi - \xi_c}{\tau - \tau_c} = (n-1)(2\sigma_1 - 1) - n\sigma_1 \left( \frac{\tau - \tau_c}{\tau_i - \tau_c} \right)^{-2/n} \quad (\text{B-18})$$



This gives  $\xi(\tau)$  on Line D. A special case is the point  $(1, \tau_L)$ :

$$\frac{1-\xi_c}{\tau_L-\tau_c} = (n-1)(2\sigma_1-1) - n\sigma_1 \left( \frac{\tau_L-\tau_0}{\tau_L-\tau_c} \right)^{-2/n} \quad (B-19)$$

Elimination of  $\xi$  between Equation (B-16) and Equation (B-18) gives  $\sigma(\tau)$  along D,

$$\frac{\sigma}{\sigma_1} = \left( \frac{\tau-\tau_0}{\tau_L-\tau_c} \right)^{-2/n} \quad (B-20)$$

The terminal value is  $\sigma_L = \sigma_2 = 2\sigma_1-1$ , or

$$\frac{\tau_L-\tau_0}{\tau_L-\tau_c} = \left( \frac{\sigma_1}{2\sigma_1-1} \right)^{n/2} \quad (B-20a)$$

The necessary equations are now at hand. Their use is as follows. The desired parameter  $\sigma_1$  is chosen and the value of  $A_m/A_1$  needed to achieve it calculated from Equation (B-11). Equation (B-13) is used to get  $\xi_1$  and  $\tau_1$ , and these, with  $\sigma_1$ , are used in Equation (B-17, B-20) to get  $\xi_0, \tau_0, \tau_L$ . Finally  $\sigma_2$  is computed as  $2\sigma_1-1$ . The desired  $\sigma(\tau)$  relationship at  $\xi = 1$  is given by  $\sigma_2(\tau_L)$ . If it is desired,  $\sigma(\xi, \tau)$  is obtained as follows:

- (a) In region bounded by A, B, and C: Equation (B-12),  $1 > \sigma > \sigma_1$
- (b) In region bounded by D, E, and F: Equation (B-16),  $\sigma_1 > \sigma > \sigma_2$
- (c) Along Line C: Equation (B-13),  $1 > \sigma > \sigma_1$
- (d) Along Line D: Equation (B-18, B-20),  $\sigma_1 > \sigma > \sigma_2$

The entire region where the waves overlap can be determined by Steps (c) and (d) above by assuming intermediate values of  $\sigma_1$  between 1 and the value of particular interest.

#### Process at the Tube End.

Here the relationship  $\sigma_2(\tau_L)$  is represented as  $\sigma(\tau)$  for intermediate values along  $\xi = 1$ , from  $\tau = 1$  to a terminal value  $\tau_L$  corresponding to the  $\sigma_1$  of interest. Of primary interest is  $p(t)$  at the end of the tube for a given  $\sigma_1$ . From Equation (B-1),

$$\frac{d \ln p}{d \ln \sigma} = n+1, \quad \frac{d \ln p}{d t} = (n+1) \frac{a_0}{L} \frac{d \ln \sigma}{d \tau} \quad (B-21)$$

As the  $\sigma(\tau)$ , or  $\sigma_2(\tau_L)$ , relationship is given by the solution of the equations derived previously,  $p(t)$  can be determined.

#### Accuracy of the "Centered Wave" Theory.

As mentioned previously, Rudinger [12] has shown that if the incident wave is centered, the reflected wave is not. The exact solution for the region where the waves overlap can be obtained with Riemann's method of characteristics. The calculation involves the hypergeometric function, which can be represented, for integral values of  $n/2$ , by a finite series with  $n/2$  terms.

Table B-1 gives values of  $\tau_L(\sigma_1)$  computed both by the "centered wave" theory developed here and by the exact method. It will be noted that the error in time of expansion is given in the last column.

There are three limits imposed on values of  $\sigma_1$ . In a shock tube driver section, the minimum value is 0.500 [12]. In the rarefaction tube as described here, its minimum is  $(n-1)/n$ . The third limit is set arbitrarily by the assumption that  $p_2/p_0$  need not be less than 0.3 (70 per cent pressure drop) in the experiments to be performed. Then the minimum  $\sigma_1$  is

$$(\sigma_1)_{\min} = (2\tau_1 - 1)_{\min} = \left( \frac{p_2}{p_0} \right)^{\frac{1}{1+n}}$$

$$(\sigma_1)_{\min} = \frac{1}{2} \left[ 1 + (0.3)^{\frac{1}{1+n}} \right]$$

These limits are tabulated below.

		Theor. Limit	Practical Limit
<u>n</u>	<u><math>\gamma</math></u>	<u><math>\sigma_1 = \frac{n-1}{n}</math></u>	<u><math>\sigma_1 = \frac{1}{2} \left[ 1 + (0.3)^{\frac{1}{1+n}} \right]</math></u>
4	5/3	0.750	0.893
6	7/5	0.833	0.921
8	9/7	0.875	0.937
10	11/9	0.900	0.948
12	13/11	0.917	0.956
14	15/13	0.923	0.961

At the limiting  $\sigma_1$  values given above, it is seen from Table B-1 that the time error at the theoretical limit is of the order of 3 per cent; at the practical limit, less than 1 per cent.

It is concluded that the centered wave theory, giving  $\tau_L(\sigma_1)$  values well within the limits of experimental accuracy for the conditions employed in experimentation, is an adequate substitute for the more cumbersome exact theory. The conclusion is supported by the facts that the first of the initial assumptions is definitely poor for large fractional pressure drops and the fifth is questionable.

#### Experimental Confirmation.

Rarefaction tests have been made in both a 4-inch tube (see Section IV) and a 1-inch tube, with  $A_m/A_o$  and  $L$  varied over wide ranges. Variation in  $n$  and  $a_o$  was achieved by the use of air and helium. Equation (B-11) is considered amply verified. Excellent agreement between predicted and observed  $\tau_L(\sigma_1)$  values is also found when  $\sigma_1$  does not crowd the practical limit and the tube length is not greater than about 60 diameters.

When the value of  $\sigma_1$  approaches the practical limit ( $M_1$  about 0.5) or the tube is long, wall friction resisting the flow of Zone 1 gas is significant. It has been found that a good first-order correction to  $p_2$  at the foot of the rarefaction can be made by assuming that the conventional pipe friction equations apply, the pressure at the mid-point of Zone 1 being the value predicted for the assigned  $\sigma_1$ .

TABLE NO. B-1  
COMPARISON OF CENTERED WAVE THEORY TO EXACT THEORY

$\gamma$	$n$	$\sigma_1$	Centered Wave $(\tau_L)_{cw}$	Exact $(\tau_L)_{ex}$	Percentage Error $100 \times \frac{(\tau_L)_{cw} - (\tau_L)_{ex}}{(\tau_L)_{ex} - 1}$
5/3	4	0.950	1.24144	1.24143	--
		0.900	1.60185	1.60156	0.05
		0.850	2.17479	2.17201	0.2
		0.800	3.16667	3.14815	0.9
7/5	6	0.950	1.39476	1.39467	--
		0.900	2.10477	2.10183	0.3
		0.850	3.53710	3.49563	1.7
9/7	8	0.950	1.57575	1.57531	0.08
		0.900	2.83745	2.81916	1.0
		0.850	6.21058	5.90322	6.3
11/9	10	0.975	1.30946	1.30941	0.02
		0.950	1.79013	1.78877	0.17
		0.900	3.93148	3.85858	2.6
13/11	12	0.950	2.04510	2.04155	0.34
		0.900	5.62044	5.37461	5.6
15/13	14	0.950	2.34965	2.34152	0.6
		0.925	4.13751	5.04529	3.0

APPENDIX C - TABLES

TABLE NO. II

SUMMARY OF PROPELLANT PROPERTIES

<u>Propellant</u>	<u>A</u>	<u>B</u>	<u>C</u>	<u>D</u>
Density lb/ft <sup>3</sup>	109	106	106	95.4
Heat Capacity* Btu/(lb)(°F)	0.30	.30	.31	0.40
Thermal Diffusevity ft <sup>2</sup> /hr	$6.5 \times 10^{-3}$	$5.4 \times 10^{-3}$	$7.6 \times 10^{-3}$	$7.6 \times 10^{-3}$
Thermal Responsivity ( $\Gamma$ ) as (kpc) <sup>1/2</sup> Btu/(hr) <sup>1/2</sup> ft <sup>2</sup> °F	2.64	2.56	2.86	3.32
Oxidizer Crystal	(NH <sub>4</sub> ) <sub>2</sub> ClO <sub>4</sub>	(NH <sub>4</sub> ) <sub>2</sub> ClO <sub>4</sub>	(NH <sub>4</sub> ) <sub>2</sub> ClO <sub>4</sub>	NH <sub>4</sub> NO <sub>3</sub>
Fuel Binder	Polysulfide	Polyurthane	ED/MVP rubber	

\*This is a calculated value based upon literature values for heat capacities of the oxidizer crystals and measured fuel-binder heat capacities.

TABLE NO. III  
SUMMARY OF PROPELLANT IGNITION DATA FROM HIGH  
TEMPERATURE, ATMOSPHERIC FURNACE

Initial Propellant Temperature  $26 \pm 2$  °C

Propellant	Furnace Temp. °K*	Ignition Time ( $\theta_i$ ) Sec.	No. of Samples	RMS Deviation Sec.	$\theta_i^{1/2}$ Sec. $^{1/2}$	Furnace Flux Btu/(sec)(ft <sup>2</sup> )
A	1005	19.10	12	0.80	4.37	5.1
A	1201	4.77	12	0.16	2.18	10.4
A	1403	1.62	10	0.04	1.27	19.3
A	1595	0.64	11	0.02	0.80	32.4
A	1785	0.35	8	0.05	0.59	50.9
B	1201	4.65	11	0.30	2.16	10.4
B	1403	1.61	13	0.06	1.27	19.3
B	1595	0.58	13	0.02	0.76	32.4
B	1785	0.29	9	0.04	0.54	50.9
C	1201	4.54	10	0.06	2.13	10.4
C	1403	1.55	18	0.07	1.25	19.3
C	1595	0.55	11	0.04	0.74	32.4
C	1785	0.20	8	0.06	0.45	50.9
D	1201	8.71	6	0.13	2.95	10.4
D	1403	2.97	14	0.08	1.72	19.3
D	1595	1.49	11	0.08	1.22	32.4
D	1785	0.74	10	0.04	0.86	50.9

\*This temperature includes a correction to make the thermocouple reading agree with a U. S. Bureau of Standards calibrated thermocouple.

TABLE NO. IV

IGNITION DATA FOR A PROPELLANT IN HIGH  
TEMPERATURE, ATMOSPHERIC FURNACE

Propellant Temp. °C	Furnace Temp °K	Ignition Time ( $\theta_i$ ) Sec.	No. of Samples	Average Deviation Sec.	$\theta_i^{1/2}$ Sec. <sup>1/2</sup>	Furnace Flux Btu/(sec) <sup>2</sup> (ft <sup>2</sup> )	Calculated T <sub>si</sub> * °C
60	1083	8.78	5	0.06	2.96	6.9	371
60	1283	2.73	6	0.10	1.65	13.5	405
60	1483	0.96	6	0.02	0.98	24.1	425
60	1685	0.41	6	0.01	0.64	40.4	458
30	1083	10.38	5	0.14	3.22	6.9	369
30	1283	3.20	6	0.05	1.79	13.5	406
30	1483	1.14	9	0.07	1.07	24.1	427
30	1685	0.47	5	0.02	0.69	40.4	457
0	1083	13.40	5	0.24	3.66	6.9	385
0	1283	3.78	4	0.10	1.94	13.5	406
0	1483	1.25	5	0.02	1.12	24.1	417
0	1685	0.54	5	0.02	0.73	40.4	458
-30	1083	14.94	5	0.15	3.87	6.9	376
-30	1283	4.57	5	0.13	2.14	13.5	414
-30	1483	1.64	5	0.02	1.28	24.1	447
-30	1685	0.69	6	0.01	0.83	40.4	468
-60	1083	17.80	5	0.70	4.22	6.9	384
-60	1283	5.40	5	0.10	2.32	13.5	425
-60	1483	1.94	4	0.02	1.39	24.1	459
-60	1685	0.85	6	0.02	0.92	40.4	481

\*Calculated for  $\Gamma = 2.64 \text{ Btu}/(\text{hr})^{1/2}(\text{ft}^2)(^\circ\text{F})$  and a surface flux equal to 90% of black body flux.

TABLE NO. V

SUMMARY OF A PROPELLANT IGNITION DATA FROM LOW  
TEMPERATURE, SEALED FURNACE

Initial Propellant Temperature  $26 \pm 1$  °C; All Tests in  
Air or Nitrogen

<u>Furnace Pressure Atms</u>	<u>Furnace Temp. °K</u>	<u>Ignition Time (<math>\theta_i</math>) Sec.</u>	<u>Nc. of Samples</u>	<u>Average Deviation Sec.</u>	<u><math>\theta_i^{1/2}</math> Sec.<sup>1/2</sup></u>
0.18	908	52.25	5	5.3	7.23
0.18	1125	10.34	5	1.1	3.22
0.18	1248	5.62	5	0.27	2.37
0.18	1347	3.31	5	0.13	1.818
0.52	908	44.3	5	3.3	6.65
0.52	1125	9.85	5	0.55	3.14
0.52	1248	5.38	5	0.12	2.32
0.52	1347	2.89	5	0.23	1.698
0.85	908	40.4	5	1.8	6.36
0.85	1125	9.14	5	0.57	3.02
0.85	1248	4.71	5	0.25	2.17
0.85	1347	2.62	5	0.17	1.617
4.25	908	28.6	5	0.94	5.34
4.25	1125	6.75	5	0.10	2.60
4.25	1248	3.48	5	0.21	1.87
4.25	1347	2.23	5	0.10	1.494
11.05	908	23.55	5	1.45	4.86
11.05	1125	6.16	5	0.40	2.48
11.05	1248	3.08	5	0.44	1.75
11.05	1347	2.08	5	0.23	1.442



TABLE NO. VI

SUMMARY OF B PROPELLANT IGNITION DATA FROM  
LOW TEMPERATURE, SEALED FURNACE

Initial Propellant Temperature  $26 \pm 1$  °C; All Tests

In Air or Nitrogen

<u>Furnace Pressure Atms</u>	<u>Furnace Temp. °K</u>	<u>Ignition Time (<math>\theta_i</math>) Sec.</u>	<u>No. of Samples</u>	<u>Average Deviation Sec.</u>	<u><math>\theta_i^{1/2}</math> Sec.<sup>1/2</sup></u>
0.18	1000	21.81	3	0.21	4.67
0.18	1125	17.81	3	0.51	4.22
0.52	1000	23.20	2	0.20	4.82
0.52	1125	9.27	3	0.47	3.08
0.52	1347	2.47	3	0.11	1.57
0.85	1000	18.12	3	0.73	4.26
0.85	1125	8.13	3	0.16	2.85
0.85	1347	2.33	3	0.26	1.53
4.25	1,000	17.52	3	1.63	4.19
4.25	1125	7.60	3	0.31	2.76
4.25	1347	2.00	3	0.15	1.41
11.05	1000	12.98	3	0.29	3.60
11.05	1125	5.92	3	0.15	2.43

TABLE NO. VII

SUMMARY OF C PROPELLANT IGNITION DATA  
FROM LOW TEMPERATURE, SEALED FURNACE

Initial Propellant Temperature  $26 \pm 1$  °C; All

Tests in Air or Nitrogen

<u>Furnace Pressure Atms</u>	<u>Furnace Temp. °K</u>	<u>Ignition Time (<math>\theta_i</math>) Sec.</u>	<u>No. of Samples</u>	<u>Average Deviation Sec.</u>	<u><math>\theta_i^{1/2}</math> Sec.<sup>1/2</sup></u>
0.18	908	60.8	5	3.6	7.79
0.18	1125	7.97	5	0.64	2.82
0.18	1248	4.07	5	0.43	2.44
0.18	1347	1.79	5	0.14	1.34
0.52	908	54.2	5	7.9	7.36
0.52	1125	8.17	5	0.77	1.60
0.52	1248	3.33	5	0.24	1.83
0.52	1347	1.84	5	0.02	1.36
0.85	908	50.4	5	2.6	7.09
0.85	1125	8.22	5	0.94	2.87
0.85	1248	3.30	5	0.31	1.82
0.85	1347	1.94	5	0.06	1.39
4.25	908	40.8	5	3.7	6.39
4.25	1125	7.40	5	0.28	2.72
4.25	1248	3.34	5	0.22	1.83
4.25	1347	1.74	5	0.07	1.32
11.05	908	30.4	5	1.0	5.51
11.05	1125	7.21	5	0.26	2.68
11.05	1248	3.44	5	0.08	1.86
11.05	1347	1.85	5	0.06	1.36

TABLE NO. VIII

SUMMARY OF D PROPELLANT IGNITION DATA  
FROM LOW TEMPERATURE, SEALED FURNACE

Initial Propellant Temperature  $26 \pm 1$  °C; All  
Tests in Air or Nitrogen

<u>Furnace Pressure Atms</u>	<u>Furnace Temp. °K</u>	<u>Ignition Time (<math>\theta_i</math>) Sec.</u>	<u>No. of Samples</u>	<u>Average Deviation Sec.</u>
0.85	1000	38.2	5	2.04
0.85	1125	12.6	5	0.65
0.85	1248	7.13	6	0.33
0.85	1357	4.13	6	0.22
2.55	1000	29.5	6	1.30
2.55	1125	10.0	8	0.54
2.55	1248	5.35	5	0.13
2.55	1357	2.93	6	0.14
4.25	1000	24.4	6	1.80
4.25	1125	10.31	6	0.61
4.25	1248	5.13	5	0.76
4.25	1357	2.80	5	0.18

TABLE IX

## IGNITION OF C PROPELLANT IN AIR - 3/8" ORIFICE

Run No.	627-6	627-7	627-8	628-1	628-2	628-3	628-4	629-1	629-2	629-3	629-4	718-2	718-3	718-4	718-5	718-6
$M_1$	2.30	2.46	2.70	3.01	3.43	3.51	3.68	3.52	3.26	3.05	3.83	2.26	2.73	3.09	3.17	3.44
$P_o$ psia	248	243	248	255	258	255	243	145	151	151	133	338	338	328	338	318
% Driver Air	19.0	14.1	9.7	6.1	3.1	0.8	0.7	1.0	3.3	6.7	1.1	13.9	9.8	6.7	3.3	0.6
$P_4$ psia	171	160	150	145	142	156	130	80	90	85	80	215	190	185	186	180
$P_4$ psia	199	192	200	200	195	198	184	111	120	111	102	260	258	254	241	240
$T_4$ °K	949	1060	1240	1460	1760	1790	1990	1850	1620	1470	2020	937	1260	1530	1570	1790
$\theta_1$ msec	n.i.	n.i.	6.8	4.8	3.2	2.3	2.9	5.0	7.6	9.2	5.8	6.0	5.4	2.9	2.7	2.1
$(T_o)$ °K	304	304	305	302	303	305	305	304	305	306	302	304	306	307	308	309
$h$ BTU/hr ft <sup>2</sup> °F	514	618	498	479	465	476	433	293	318	302	272	636	605	584	558	549
$\theta_1$ msec <sup>1/2</sup>	n.i.	n.i.	2.6	2.2	1.8	1.5	1.7	2.2	2.8	3.0	2.4	2.5	2.3	1.7	1.6	1.4
$\Delta T_1$ °K			255	287	300	267	303	197	266	245	270	204	283	285	276	290
$q$ BTU/sec ft <sup>2</sup>			179	224	300	312	316	162	171	144	200	142	216	297	308	357

TABLE X

## IGNITION OF C PROPELLANT IN AIR - 5/16" ORIFICE

Run No.	<u>615-1</u>	<u>616-1</u>	<u>616-2</u>	<u>616-3</u>	<u>616-4</u>	<u>617-1</u>	<u>630-1</u>	<u>630-2</u>	<u>701-1</u>	<u>701-2</u>	<u>709-1</u>	<u>709-2</u>
$M_1$	3.46	2.97	2.73	2.53	2.33	3.79	3.00	3.11	3.20	3.62	3.34	3.55
$P_o$ psia	243	243	248	248	273	248	128	128	143	193	147	161
% Driver Air	0.8	6.6	9.7	13.8	17.3	0.7	1.9	1.7	1.7	1.0	3.4	1.3
$P_4$ psia	145	140	145	168	185	145	77	80	--	110	85	100
$P_4'$ psia	183	183	191	213	218	188	107	100	100	142	115	125
$T_4'$ °K	1730	1410	1250	1110	973	2030	1460	1500	1470	1900	1680	1820
$\theta_i$ msc	6.5	7.4	10.0	7.0	n.i.	3.6	10.0	n.i.	n.i.	5.0	6.3	7.0
$(T_1)_o$ °K	300	302	303	303	304	303	305	305	305	306	303	304
$h$ BTU/hr $ft^2$ °F	332	336	364	399	412	333	216	207	185	265	221	244
$\theta_i^{\frac{1}{2}}$ msc $^{\frac{1}{2}}$	2.6	2.7	3.2	2.7	n.i.	1.9	3.2	n.i.	n.i.	2.2	2.5	2.6
$\Delta T_i$ °K	275	226	243	197		269	182			236	192	246
$q$ BTU/sec $ft^2$	191	155	104	132		251	107			197	136	165

TABLE X (Cont.)

Run No.	<u>714-1</u>	<u>714-2</u>	<u>714-3</u>	<u>714-4</u>	<u>714-5</u>	<u>714-6</u>	<u>714-7</u>	<u>715-1</u>	<u>715-2</u>	<u>718-1</u>	<u>615-2</u>
$M_1$	2.04	2.59	2.62	2.78	2.81	2.71	2.91	3.04	3.11	3.18	3.13
$P_o$ psia	361	363	363	358	288	355	313	313	303	353	238
% Driver Air	18.0	18.0	9.1	9.4	7.7	6.2	7.0	3.5	3.8	0.6	3.4
$P_4$ psia	238	230	208	200	160	196	185	170	184	189	135
$P_4'$ psia	275	290	284	278	215	262	249	239	238	260	178
$T_4'$ °K	797	1150	1190	1320	1330	1270	1400	1490	1500	1570	1520
$\theta_1$ msc	8.5	4.4	4.4	3.2	4.8	3.9	3.9	n.i.	5.2	2.3	6.7
$(T_1)_o$ °K	303	303	303	307	308	308	308	304	305	304	301
$h$ BTU/hr $ft^2$ °F	481	501	490	474	387	455	430	410	414	440	323
$\theta_1^{\frac{1}{2}}$ msc $^{\frac{1}{2}}$	2.9	2.1	2.1	1.8	2.2	2.0	2.0	n.i.	2.3	1.5	2.6
$\Delta T_1$ °K	87	207	214	198	208	204	226		266	217	245
$q$ BTU/sec $ft^2$	54	176	183	197	170	184	205		207	254	168

TABLE XI

## IGNITION OF C PROPELLANT IN AIR - 1/4" ORIFICE

Run No.	623-1	623-2	623-3	627-1	627-2	627-3	627-4	627-5	709-3	711-1	711-2	711-3	711-4	711-5	712-5	713-1	713-2
$M_L$	3.71	3.57	3.67	2.99	3.18	2.81	2.49	2.24	3.59	3.38	3.88	3.02	3.22	3.51	2.75	2.57	2.35
$P_o$ psia	268	255	260	257	243	258	253	255	157	158	155	358	348	328	338	318	343
% Driver Air	0.6	0.8	0.7	3.1	6.6	9.7	13.5	18.5	1.4	3.2	1.0	6.2	3.9	0.6	9.8	14.8	19.0
$P_4$ psia	155	142	153	155	143	150	160	175	95	90	71	210	192	195	209	210	250
$P'_4$ psia	207	190	200	200	187	197	200	200	122	122	117	280	277	253	254	250	280
$T_4$ °K	1960	1820	1900	1400	1530	1290	1080	908	1870	1710	2210	1450	1610	1800	1250	1140	975
$\theta_1$ msec	9.0	4.2	5.2	4.2	9.8	6.8	8.5	n.i.	6.0	n.i.	n.i.	2.4	2.4	1.4	3.4	5.4	n.i.
$(T_1)_o$ °K	297	297	298	299	300	301	301	303	305	299	301	301	302	304	305	306	307
$h$ BTU/hr ft <sup>2</sup> °F	237	223	231	241	224	241	251	259	157	155	145	312	306	283	298	298	333
$\theta_f$ msec	3.0	2.1	2.3	2.1	3.1	2.6	2.9	n.i.	2.4	n.i.	n.i.	1.6	1.6	1.2	1.8	2.3	n.i.
$\Delta T_1$ °K	336	191	236	150	220	162	143		160			186	228	163	144	149	
$q$ BTU/sec ft <sup>2</sup>	198	165	176	129	124	120	88		115			213	224	162	139	114	

TABLE XII

## IGNITION OF C PROPELLANT IN NITROGEN

<u>Run No.</u>	<u>802-4</u>	<u>802-5</u>	<u>802-6</u>	<u>803-1</u>	<u>803-2</u>	<u>803-3</u>
Orifice	5/16"	5/16"	5/16"	3/8"	3/8"	3/8"
$M_1$	3.29	3.01	3.54	2.81	2.57	3.25
$P_o$ psia	268	258	242	258	268	262
% Driver Air	3.0	6.2	0.8	9.3	12.7	3.1
$P_4$ psia	150	145	135	150	172	150
$P_4'$ psia	207	202	190	202	215	210
$T_4'$ °K	1649	1460	1859	1300	1121	1620
$\theta_i$ msec	4.5	6.5	5.4	5.2	9.9	4.6
$(T_1)_o$ °K	302	303	304	300	301	301
$h$ BTU/hr ft <sup>2</sup> °F	368	365	337	493	537	493
$\theta_i^{\frac{1}{2}}$ msec <sup><math>\frac{1}{2}</math></sup>	2.1	2.6	2.3	2.3	3.2	2.1
$\Delta T_i$ °K	256	255	295	252	196	317
$q$ BTU/sec ft <sup>2</sup>	213	178	226	196	108	262



TABLE XIII

## IGNITION OF A PROPELLANT IN AIR

Run No.	<u>728-1</u>	<u>728-2</u>	<u>728-3</u>	<u>728-4</u>	<u>728-5</u>	<u>728-6</u>	<u>728-7</u>
Orifice	5/16"	5/16"	5/16"	5/16"	1/4"	1/4"	3/8"
$M_1$	2.86	3.07	3.41	3.38	3.47	3.50	3.50
$P_o$ psia	312	288	302	288	312	342	338
% Driver Air	7.1	3.8	0.7	0.7	0.6	0.6	0.6
$P_4$ psia	188	170	180	177	175	200	191
$P_4'$ psia	245	230	232	230	245	260	250
$T_4'$ °K	1337	1487	1729	1711	1811	1805	1813
$\theta_i$ msec	n.i.	10.0	7.2	9.0	9.2	7.6	3.7
$(T_1)_o$ °K	303	303	304	305	305	306	307
$h$ BTU/hr ft <sup>2</sup> °F	433	400	398	397	267	285	581
$\theta_i^{\frac{1}{2}}$ msec <sup><math>\frac{1}{2}</math></sup>	n.i.	3.2	2.7	3.0	3.0	2.8	1.9
$\Delta T_i$ °K		304	320	356	298	272	343
$q$ BTU/sec ft <sup>2</sup>		187	232	231	191	191	347
		3 msec after rare- fac- tion		2 msec after rare- fac- tion	3 msec after rare- fac- tion	igni- tion coin- cides with rare- fac- tion	

TABLE XIV

## IGNITION OF A PROPELLANT IN OXYGEN

Run No.	801-6	823-1	823-2	823-3	823-4	824-1	824-2	824-3	824-4	824-5	824-6
Orifice	5/16"	1/4"	1/4"	1/4"	5/16"	5/16"	3/8"	3/8"	3/8"	3/8"	3/8"
$M_1$	3.21	3.10	3.17	3.43	3.15	3.47	3.12	3.46	3.47	3.52	3.43
$P_o$ psia	260	237	262	257	257	254	247	254	300	323	341
% Driver Air	3.1	3.4	3.1	0.8	3.2	0.8	3.2	0.8	0.7	0.6	0.6
$P_4$ psia	159	142	158	142	155	150	145	151	175	190	200
$P_4'$ psia	205	192	208	202	207	200	197	195	225	240	255
$T_4'$ °K	1580	1457	1504	1731	1510	1727	1481	1711	1707	1754	1695
$\Theta_1$ msec	6.9	n.i.	n.i.	8.0	6.3	6.3	n.i.	4.2	5.0	4.0	3.4
$(T_1)_o$ °K	305	294	295	297	298	294	295	296	293	295	298
$h$ BTU/hr $ft^2$ °F	367	230	245	235	372	353	476	468	524	541	581
$h\Delta T_{1n}$ BTU/sec $ft^2$	190		127		177	205		271	299	323	332
$\Theta_1^{\frac{1}{2}}$ msec $^{\frac{1}{2}}$	2.6		2.8		2.5	2.5		2.1	2.2	2.0	1.8
	Extinguished by rarefaction		Ignition coincided with rarefaction		Ignited, extinguished, reignited	Ignited, extinguished, reignited	Apparently ignited by a subsequent shock wave				

TABLE XV  
IGNITION OF B PROPELLANT IN AIR

<u>Run No.</u>	<u>728-8</u>	<u>730-1</u>	<u>730-2</u>
Orifice	3/8"	5/16"	1/4"
$M_1$	3.52	3.52	3.57
$P_o$ psia	338	338	366
% Driver Air	0.6	0.6	0.5
$P_4$ psia	208	202	200
$P_4'$ psia	280	265	284
$T_4'$ °K	1849	1804	1886
$\theta_i$ msec	3.2	2.0	2.2
$(T_1)_o$ °K	308	303	304
$h$ BTU/hr ft <sup>2</sup> °F	615	441	304
$\theta_i^{\frac{1}{2}}$ msec <sup><math>\frac{1}{2}</math></sup>	1.8	1.4	1.5
$\Delta T_i$ °K	365	225	193
$q$ BTU/sec ft <sup>2</sup>	391	314	255

TABLE XVI

## IGNITION OF B PROPELLANT IN OXYGEN

<u>Run No.</u>	<u>827-3</u>	<u>827-4</u>	<u>827-5</u>	<u>827-6</u>	<u>827-7</u>
Orifice	3/8"	3/8"	3/8"	3/8"	3/8"
$M_1$	3.45	3.23	3.27	3.51	2.87
$P_o$ psia	259	259	352	367	362
% Driver Air	0.8	3.1	2.8	0.5	6.0
$P_4$ psia	140	153	218	215	205
$P_4'$ psia	200	198	272	288	270
$T_4'$ °K	1767	1571	1591	1801	1334
$\theta_i$ msc	4.5	6.3	3.0	2.0	2.47
$(T_i)_o$ °K	299	300	301	302	302
$h$ BTU/hr ft <sup>2</sup> °F	573	475	611	632	628
$h\Delta T_{1n}$ BTU/sec ft <sup>2</sup>	278	244	322	400	245
$\theta_i^{\frac{1}{2}}$ msc <sup><math>\frac{1}{2}</math></sup>	2.1	2.5	1.7	1.4	2.5
	Extin- guished 10% bur- ned away	Extin- guished by rare- faction but reignited	Extin- guished by rare- faction but reignited	Extin- guished 75% bur- ned away	Extin- guished 50% bur- ned away

TABLE NO. XVII  
COMBUSTION RESPONSE TO RAREFACTIONS

<u>Propellant</u>	<u>Initial Nitrogen Pressure, psig</u>	<u>Per Cent Drop in Pressure</u>	<u>Observations at Light Signal</u>
<sup>A</sup> (AP-PS, 2% Al)	450	21	Reduced, Stable
		44	Large Reduction
	135	30	Reduced, Stable
		44	Large Reduction
<sup>B</sup> (AP-PU, 2% Al)	450	21	Reduced, Stable
		44	Out
	145	30	Out at second wave
		44	Out
<sup>C</sup> (AP-BD/MVP, no Al)	460	60	Reduced after flash
	140	54	Reduced after flash

TABLE XVIII

## SUMMARY OF INITIAL SURFACE TEMPERATURE RISE

Rectangular Section 1 7/8-inch Shock Tube

Run No.	$M_E$	$\Delta T_c \frac{(P^*)^{\frac{1}{2}}}{(P_4)}$	$\Delta T_o \frac{(P^*)}{(P_4)}$ Adjusted for $\Gamma$	
717-5	2.02	14.5	11.7	Orifice No. 3 Gage No. 4 (Glass) Driver Press. (150 psig)
717-7	2.06	14.2	11.4	
717-8	2.16	13.6	10.9	
718-1	2.03	14.3	11.5	
718-2	2.56	20.1	16.2	
718-4	2.34	23.0	18.5	
718-5	2.52	21.9	17.6	
718-7	2.50	20.5	16.5	
718-8	2.73	21.9	17.6	
718-12	2.70	21.5	17.3	
719-1	2.84	22.3	17.9	
719-5	2.96	22.6	18.2	Orifice No. 3 Gage No. 4 (Glass) Driver Press. 250 psig
719-6	3.32	27.0	21.7	
719-7	3.22	26.4	21.2	
719-8	3.35	24.2	19.5	
719-10	3.93	26.0	20.9	
719-9	3.86	26.0	20.9	
720-4	2.02	15.6	12.6	
722-1	1.99	13.8	11.1	
722-2	2.23	21.7	17.6	
722-5	2.50	20.0	16.1	
722-6	2.94	28.2	22.7	
722-7	2.90	26.0	20.9	
722-8	3.29	43.2	34.8	Orifice No. 3 Gage No. 4 (Glass) Driver Pressure 350 psig
722-9	3.72	37.6	30.2	
724-1	3.74	30.4	24.5	
725-2	3.87	44.0	35.4	
724-3	2.20	22.8	18.3	
724-4	2.42	24.9	20.0	
728-1	3.42	32.5	26.2	
724-5	2.40	24.9	20.0	
724-6	3.38	36.5	29.4	
727-1	3.42	35.2	28.3	
728-2	3.32	35.1	28.2	
728-3	1.92	13.4	10.8	Orifice No. 5 Gage No. 4 Driver Press. 150 psig
728-4	1.93	13.7	11.0	
729-1	2.66	20.4	16.4	
729-2	3.44	27.2	21.9	
731-1	1.94	15.4	12.4	Orifice No. 2 Gage No. 4 Driver Press. 150 psig
731-2	1.88	14.2	11.4	
731-3	2.60	24.3	19.5	
731-4	2.68	24.4	19.6	
731-5	3.39	32.7	26.3	

TABLE XVIII (Cont.)

Run No.	$M_E$	$\Delta T_o \left( \frac{P^*}{P_4} \right)^{\frac{1}{2}}$	$\Delta T_o \left( \frac{P^*}{P_4} \right)$ Adjusted for $\Gamma$	
731-6	1.93	15.0	12.1	Orifice No. 1 Gage No. 4 Driver Press. 150 psig
731-7	2.73	24.0	19.3	
82-1	3.42	31.2	25.1	
82-2	3.48	30.4	24.4	
82-4	1.94	10.5	10.4	Orifice No. 3 Gage No. 3 Driver Press. 150 psig
83-1	2.62	17.7	17.5	
85-1	2.63	18.1	17.9	
85-2	3.40	25.6	25.3	
630-2	3.80	22.6	22.1	
85-3	1.99	13.1	12.9	Orifice No. 3 Gage No. 3 Driver Press. 250 psig
85-5	2.75	22.2	21.9	
85-6	2.75	22.2	21.9	
87-1	2.76	23.6	23.3	
87-2	1.99	2.58	11.7	Orifice No. 3 Gage No. 1 Driver Press. 150 psig
87-3	1.93	2.56	11.6	
87-4	2.69	4.02	18.3	
95-1	2.71	3.98	18.1	
95-2	2.67	4.11	18.7	
95-5	2.98	4.10	18.7	
95-6	3.38	4.49	20.4	
95-7	2.00	2.68	12.2	Orifice No. 3 Gage No. 1 Driver Press. 250 psig
95-8	2.03	2.70	12.3	
95-9	2.78	4.19	19.0	
96-1	2.88	4.95	22.5	
918-5	2.77	4.65	21.2	
96-3	2.21	4.03	18.4	Orifice No. 3 Gage No. 1 Driver Press. 250 psig
96-4	2.19	3.68	16.8	
96-5	3.40	5.71	26.0	
96-6	2.27	4.17	19.0	
918-2	2.20	4.12	18.7	
918-3	2.42	4.18	19.1	
918-4	3.49	5.94	27.0	

TABLE XIX

## SUMMARY OF NOZZLE HEAT TRANSFER DATA

Driven Gas: Air Rectangular Test Section

1 7/8-inch Shock Tube

Run No.	Heat Flux Gage	$M_E$	$P_4$ (psia)	$\Delta T_{\infty} \left( \frac{P^*}{P_4} \right)^{\frac{1}{2}}$ (°K)	$P_4'$ (psia)	$T_4'$ (°K)	$h$ $\frac{\text{Btu}}{\text{hr ft}^2 \text{ } ^\circ\text{F}}$	$G$ $\frac{\text{lb}}{\text{sec ft}^2}$	$h/(T_4')^{0.3}$ $\frac{\text{Btu}}{\text{hr ft}^2 \text{ } ^\circ\text{R}^{1.3}}$
718-1	Glass	2.03	128	14.3	152	812	189	71.5	21.2
718-8	Glass	2.73	111	21.9	148	1290	157	54.6	15.4
719-8	Glass	3.35	93	24.2	146	1770	141	45.6	12.6
720-4	Glass	2.02	192	15.6	232	808	306	112	34.2
722-7	Glass	2.90	173	26.0	243	1400	250	85.4	24.0
722-8	Glass	3.29	172	43.2	238	1670	348	77.9	32.8
724-3	Glass	2.20	238	22.8	327	915	420	146	45.6
728-1	Glass	3.42	244	32.5	325	1720	307	103.2	27.4
728-2	Glass	3.32	236	35.1	323	1650	298	105	27.1
82-4	Pyro-ceram	1.94	121	10.5	148	724	249	70.4	30.2
85-1	Pyro-ceram	2.63	111	18.1	145	1135	183	58.0	19.5
85-2	Pyro-ceram	3.40	107	25.6	136	1700	211	43.2	18.8
85-3	Pyro-ceram	1.99	199	13.1	238	784	314	114	35.7
85-5	Pyro-ceram	2.75	170	22.2	232	1282	264	86.1	26.4
87-3	Alumina	1.93	120	2.56	139	736	208	69.0	24.1
87-4	Alumina	2.68	115	4.02	148	1221	191	55.1	19.0



TABLE XX

## SUMMARY OF NOZZLE HEAT TRANSFER DATA

Driven Gas: Air      Triangular Test Section  
4-inch Shock Tube      Heat-Flux Gage Substrate

Run No.	$M_1$	$P_4'$ psia	$T_4'$ °K	$G$ #/sec ft <sup>2</sup>	$h$ BTU/hr ft <sup>2</sup> °F	$h/T_4^{1.3}$ BTU/hr ft <sup>2</sup> °F <sup>1.3</sup>	$\Gamma^*$ BTU/hr ft <sup>2</sup> °F
421-1	2.50	131	1040	128	424	44.5	0.178
422-1	2.53	134	1110	126	434	44.2	0.167
422-2	3.09	122	1480	102	389	36.3	0.138
422-3	2.45	114	1020	49	190	20.1	0.153
426-1	2.49	134	1040	57	202	21.3	0.172
427-6	2.55	144	1110	59	198	20.2	0.168
427-2	3.02	144	1458	52	230	21.9	0.146
504-1	3.45	121	1705	40	219	19.5	0.132
504-2	3.88	116	2110	34	240	20.3	0.087
505-2	2.51	134	1050	89	338	34.8	0.164
505-3	2.96	129	1420	74	307	29.8	0.131
506-1	3.44	123	1732	65	298	26.6	0.129
506-2	4.02	118	2330	53	243	19.3	0.082
506-3	3.17	129	1515	106	438	40.9	0.145
506-4	3.47	124	1780	94	374	32.8	0.123
509-1	3.88	120	2190	81	327	27.3	0.097
527-1	3.14	224	1520	125	446	39.1	0.200
527-2	3.52	212	1780	110	490	43.0	0.215
527-3	3.06	240	1510	84	328	30.7	0.212
527-5	2.96	205	1380	171	652	61.6	0.241
528-1	3.60	217	1850	162	615	53.5	0.160
528-2	3.39	268	1630	90	438	39.8	0.335
528-3	3.56	285	1810	91	391	34.3	0.275
530-1	3.46	270	1690	200	540	48.6	0.231
604-1	3.00	124	1420	73	317	29.9	0.139
712-2	3.60	265	1750	130	610	54.4	0.263
712-1	2.85	252	1335	148	599	57.6	0.277
712-3	3.10	300	1555	235	785	72.0	0.257
712-4	3.54	270	1815	196	682	59.9	0.258

\*This is the effective value for air and was calculated from the initial discontinuous temperature rise. For the gage  $\Gamma$  was 5.52 BTU/(hr)<sup>1/2</sup> (ft<sup>2</sup>)<sup>1/2</sup> (°F).

# TABLE OF NOMENCLATURE

A	constant describing the reaction rate in the propellant, Equation (9)
B	constant describing the reaction rate of the surface propellant reactions, Equation (1)
C	heat capacity of propellant or heat flux gage
E	activation energy for ignition reactions, Equations (1) and (9)
f	heat flux; $f_s$ , surface heat flux; $f'$ , energy generation rate per unit surface area as a result of surface ignition reactions
G	gas mass velocity at gage or propellant surface
H	constant in Equation (9)
h	surface heat transfer coefficient
I	constant in Equation (2)
k	thermal conductivity of propellant or heat flux gage
M	incident shock wave Mach No.; $M_1$ or $M_E$ at end of shock tube
n	minus slope of $d \ln \Theta_i / d \ln p$ , Equation (13)
N	see Equation B-2
p	pressure; $p^*$ reference pressure, 100 psia; $p_4$ pressure behind incident shock wave; $p_4'$ final, maximum pressure behind incident shock wave
q'	energy generation rate per unit volume as a result of ignition reactions
R	gas constant
S	see Equation (3); $\mathcal{S}$ see Equation (10)
T	absolute temperature; $T_s$ , surface temperature; $T_{si}$ , calculated surface temperature at the ignition time; $T_o$ , initial propellant or gage temperature; $T_j$ , propellant or gage surface temperature after initial discontinuous temperature rise; $T_g$ or $T_4'$ , calculated gas temperature at $p_4'$ ; $\Delta T_o = T_j - T_o$
$\Gamma$	square root of product kpc
$\Theta$	time; $\Theta_i$ , ignition time
$\rho$	density of propellant or gage

Subscripts.

- i denotes evaluation at experimental ignition time
- o initial value
- s denotes evaluation at a surface

#### LIST OF REFERENCES

1. Beyer, R. B., and N. Fishman, Solid Propellant Ignition Studies with High Flux Radiant Energy as a Thermal Source, Solid Propellant Rocket Research, p. 673, Academic Press, New York (1960).
2. Keller, J. A., and N. W. Ryan, Measurement of Heat Flux From Initiators for Solid Propellants, ARS Jour., 31, 1375 (1961).
3. Altman, D., and A. F. Grant, Thermal Theory of Solid-Propellant Ignition by Hot Wires, Fourth Symposium on Combustion, The Williams and Wilkins Co., Baltimore, 158 (1953).
4. Hicks, B. L., Theory of Ignition Considered as a Thermal Reaction, Jour. Chem. Phys., 22, 414 (1953).
5. Baer, A. D., Ignition of Composite Rocket Propellants, Ph.D. Thesis, University of Utah, (1959).
6. Baer, A. D., N. W. Ryan, and D. L. Salt, Ignition of Composite Propellants, AFOSR TN 59-516, ASTIA No. AD 216 291 (1959).
7. Baer, A. D., N. W. Ryan, and D. L. Salt, Propellant Ignition by High Convective Heat Fluxes, Solid Propellant Rocket Research, p. 653, Academic Press, New York (1960).
8. McAlevy, R. F., P. L. Cowan, and M. Summerfield, The Mechanism of Ignition of Composite Solid Propellant Propellants by Hot Gases, Solid Propellant Rocket Research, p. 623, Academic Press, New York (1960).
9. Ciepluch, C. C., The Effect of Rapid Pressure Decay on Solid Propellant Combustion, ARS Jour., 31, 1584 (1961).
10. Vidal, R. J., Model Instrumentation Techniques for Heat Transfer and Force Measurement in a Hypersonic Shock Tunnel, Cornell Aeronautical Laboratory Report No. AD-917-A-1, WADC-TN-56-315, ASTIA No. AD-97238 (1956).
11. Boelter, L. M. K., G. Young, and H. W. Iversen, An Investigation of Aircraft Heaters XXVII - Distribution of Heat-Transfer Rate in the Entrance Section of Circular Tube, NACA TN 1451 (1948).
12. Rudinger, George, (a) Personal Communication; (b) Interaction of Centered Expansion Waves, ARS Jour., 31, 1587 (1961).
13. McCune, C. C., Solid Propellant Ignition Studies in a Shock Tube, Ph.D. Thesis, University of Utah (1961).

SOLID PROPELLANT DISTRIBUTION LIST  
AFOSR - PROPULSION RESEARCH DIVISION

20 June 1961

(Supersedes all previous lists)

ALL UNCLASSIFIED REPORTS

No. of Copies

Aerojet-General Corporation 1  
ATTN: Library  
Azusa, California

Atlantic Research Corporation 1  
ATTN: Library  
Alexandria, Virginia

Utah University 1  
ATTN: Dr. N. W. Ryan  
Salt Lake City, Utah

Princeton University 1  
ATTN: Dr. Summerfield  
Princeton, New Jersey

Lockheed Missile System 1  
ATTN: Dr. Nachbar  
Sunnyvale, California

Stanford Research Institute 1  
ATTN: Library  
Menlo Park, California

Solid Propellant Information Agency 3  
Applied Physics Laboratory  
Johns Hopkins University  
Silver Spring, Maryland

Rocketdyne Division, NAA 1  
ATTN: Dr. R. Lawhead  
Canoga Park, California

Armour Research Foundation 1  
ATTN: Dr. T. P. Torda  
10 West 35th Street  
Chicago, Illinois

BASIC GOVERNMENT DISTRIBUTION LIST  
AFOSR - PROPULSION RESEARCH DIVISION

16 May 1961

(Supersedes all previous lists)

ALL UNCLASSIFIED REPORTS

	<u>No. of Copies</u>		<u>No. of Copies</u>
ASTIA (TIPCR)	10	AFCRL (Library)	1
Arlington Hall Station		L. G. Hanscom Field	
Arlington 12, Virginia		Massachusetts	
OTS, Dept. of Commerce	1	Lewis Research Center (NASA)	1
Technical Reports Branch		ATTN: Technical Library	
Washington 25, D. C.		21000 Brookpark Road	
		Cleveland 35, Ohio	
AFOSR (SRGL)	2	Wallops Station (NASA)	1
Washington 25, D. C.		ATTN: Technical Library	
		Wallops Island, Virginia	
RAND Corporation	2	Institute of Technology (AU) Library 1	
1700 Main Street		MCLI-LIB, Bldg. 125, Area B	
Santa Monica, California		Wright-Patterson AFB, Ohio	
National Aeronautics and			
Space Administration	1	ASD (Lib)	1
ATTN: Library		Wright-Patterson AFB, Ohio	
1520 H Street, N. W.			
Washington 25, D. C.		ARGMA(ORDXR-OTL)	1
Ames Research Center (NASA)	1	Redstone Arsenal, Alabama	
ATTN: Technical Library			
Moffett Field, California		Chief, R and D, Dept. of the Army 1	
High Speed Flight Station (NASA) 1		ATTN: Scientific Information Branch	
ATTN: Technical Library		Washington 25, D. C.	
Edwards AFB, California		Institute of the Aeronautical Sciences 1	
Langley Research Center (NASA) 1		2 East 64th Street	
ATTN: Technical Library		New York 21, New York	
Langley AFB, Virginia		Applied Mechanics Reviews	2
Chairman		Southwest Research Institute	
Canadian Joint Staff (DRB/DSIS) 1		8500 Culebra Road	
2450 Massachusetts Avenue, N. W.		San Antonio 6, Texas	
Washington, D. C.		EOAR	1
Marshall Space Flight Center	1	The Shell Building	
ATTN: Library		47 Rue Cantersteen	
Huntsville, Alabama		Brussels, Belgium	
AFSC(SCRS)	1		
Andrews AFB		AFOSR (SRLTL)	1
Washington 25, D. C.		Holloman AFB, New Mexico	

AFFTC (Library)	1	Naval Bureau of Weapons	1
Edwards AFB, California		ATTN: Library	
		Washington 25, D. C.	
AEDC (Library)	1	US Atomic Energy Commission	1
Arnold AF Stn., Tennessee		Tech. Information Service	
US Naval Research Laboratory Library	1	1901 Constitution Avenue	
Washington 25, D. C.		Washington 25, D. C.	
ARL (TECHNICAL LIBRARY)	1	Commanding Officer	1
Building 450		White Sands Proving Ground	
Wright-Patterson AFB, Ohio		ATTN: Library	
		White Sands, New Mexico	
AFSWC (Library)	1		
Kirtland AFB, New Mexico			
Signal Corps Engineering Laboratory	1		
(SIGFM/EL-RPO)			
Fort Monmouth, New Jersey			
Jet Propulsion Lab (NASA)	1		
CIT, Pasadena, California			
Director, Ballistics Research Lab	1		
Aberdeen Proving Ground			
Aberdeen, Maryland			
Army Research Office	1		
Duke Station			
ATTN: CRD-AA-IP			
Durham, N. Carolina			
Naval Ordnance Laboratory	1		
ATTN: Library			
White Oak, Silver Spring			
Maryland			
National Bureau of Standards	1		
ATTN: Library			
Washington 25, D. C.			
AFSC (BSD)	1		
ATTN: Library			
AF Unit PO			
Los Angeles 45, California			
Chief of Naval Research	1		
Dept. of Navy			
ATTN: Library			
Washington 25, D. C.			
AFOSR (SRHP)	1		
OAR			
Washington 25, D. C.			